

# A VLT/FLAMES survey for massive binaries in Westerlund 1: VIII. Binary Systems and Orbital Parameters

B. W. Ritchie<sup>1,2</sup>, J. S. Clark<sup>1,\*</sup>, I. Negueruela<sup>3</sup>, and F. Najarro<sup>4</sup>

<sup>1</sup> Department of Physics and Astronomy, The Open University, Walton Hall, Milton Keynes, MK7 6AA, UK.  
e-mail: [ben.ritchie@open.ac.uk](mailto:ben.ritchie@open.ac.uk)

<sup>2</sup> Lockheed Martin Integrated Systems, Building 7000, Langstone, Hampshire, PO9 1SA, UK.

<sup>3</sup> Departamento de Física Aplicada, Facultad de Ciencias, Universidad de Alicante, Carretera de San Vicente s/n, E03690, San Vicente del Raspeig, Spain

<sup>4</sup> Centro de Astrobiología, CSIC-INTA, Ctra de Torrejón a Ajalvir km 4, E-28850 Torrejón de Ardoz, Madrid, Spain.

Received 18 October 2021 / Accepted 24 November 2021

## ABSTRACT

**Context.** The galactic cluster Westerlund 1 contains a rich population of evolved, massive stars. A high binary fraction has been inferred from previous multiwavelength observations.

**Aims.** We use multi-epoch spectroscopy of a large sample of early-type stars in Westerlund 1 to identify new binaries and binary candidates in the cluster.

**Methods.** VLT/FLAMES was used with the GIRAFFE spectrograph in HR21 mode to obtain spectra of  $\sim 100$  OB stars over a 14-month baseline in 2008 and 2009, supplemented with follow-up observations in 2011 and 2013. Radial velocities were obtained from strong Paschen series absorption lines in the *I*-band.

**Results.** We identify 20 new OB I–III binaries, a WN9h: binary, and a WC9d binary, greatly increasing the number of directly confirmed binary systems in Westerlund 1, while 12 O9–9.5 Iab–III stars are identified as candidate binaries based on radial velocity changes that are inconsistent with photospheric variability. The 173.9 day SB1 W1030 represents the first longer-period system identified in the cluster, while the determination of a 53.95 day period for W44 (WR L) makes it the first Wolf-Rayet binary in Westerlund 1 with a confirmed orbital period greater than ten days. Our results suggest the binary fraction in the OB population is at least  $\sim 40\%$ , and may be significantly higher.

**Conclusions.** These results demonstrate that binary systems can be effectively identified in the population of OB I–III stars evolving off the main sequence in Westerlund 1. Future multi-epoch surveys will be able to fully characterise this population.

**Key words.** stars: evolution - supergiants - stars: binaries: general - techniques: radial velocities

## 1. Introduction

In recent years a number of large multi-epoch spectroscopic radial velocity (RV) surveys have been carried out to characterise the high-mass binary populations in young, massive clusters ( $M \gtrsim 10^4 M_\odot$ , ages of a few Myr), focusing on both Galactic clusters and the Small and Large Magellanic clouds (e.g. Evans et al. 2008; Bosch et al. 2009; Ritchie et al. 2009a; Clark et al. 2015; Almeida et al. 2017; Lohr et al. 2018; Evans et al. 2020, and references therein). These studies are motivated by the high binary fraction amongst massive stars (Sana et al. 2012) and the critical role binary interaction plays throughout the late-stage evolution and ultimate core-collapse of such systems (Langer et al. 2003; Schneider et al. 2015), with their relativistic remnants powering a range of high-energy phenomena such as  $\gamma$ -ray bursts, high-mass X-ray and  $\gamma$ -ray binaries, and, eventually, the generation of gravitational waves from the inspiral and coalescence of neutron stars and black holes.

\* In Memoriam: This work is dedicated to the memory of Dr. Simon Clark, who tragically passed away while the paper was in preparation. His friendship and passion for Astronomy are deeply missed by all who worked with him.

In this paper, we report the full results of a study of OB stars in the very massive galactic cluster Westerlund 1 (hereafter Wd1; Westerlund 1961; Clark et al. 2005; Negueruela et al. 2010; Clark et al. 2020) with the Fibre Large Array Multi Element Spectrograph (FLAMES; Pasquini et al. 2002), based on observations obtained in 2008–2009 and supplemented with additional FLAMES observations obtained during 2011 and 2013. Although heavily reddened, the luminous stellar population of Wd1 can be observed in the *R*- and *I*-bands, revealing an apparently-coeval population of OB stars<sup>1</sup> evolving off the main sequence (MS), along with a rich population of post-MS objects that include blue supergiants (BSGs), yellow hypergiants (YHGs), red supergiants (RSGs), and Wolf-Rayet (WR) stars (Clark et al. 2010, 2020). A photometric study of the stellar population by Bonanos (2007)

<sup>1</sup> Wd1 contains a large population of  $\sim O9$  II–III stars, implying a MS turn-off around  $\sim O8$  V (Clark et al. 2020), but to date no examples of the early-B II–III stars that would trace an older stellar population evolving off the MS have been observed; in the *I*-band, such objects would be easily distinguished from the late-O population by the presence of He I and N I absorption lines and the absence of C III (Negueruela et al. 2010).

found four eclipsing binary systems with periods of less than ten days and a similar number of systems with ellipsoidal variations in their light curves suggestive of binarity, while observations at radio (Dougherty et al. 2010), infra-red (Crowther et al. 2006) and X-ray wavelengths (Skinner et al. 2006; Clark et al. 2008, 2019b) also suggest that Wd1 is binary-rich, although these wavelengths probe secondary indicators of binarity from wind interaction: X-ray emission from colliding winds (Stevens et al. 1992), an infra-red excess due to hot dust formed in a wind-interaction zone (Williams et al. 2003), or non-thermal radio spectra (De Becker & Raucq 2013).

Short-period binaries in Wd1 are expected to undergo Roche-lobe overflow as the primary evolves off the MS (Langer et al. 2003; Petrovic et al. 2005) and will become WR+O binaries without ever reaching the B–F hypergiant phase (cf. W13, W72/WR A, WR B, and W239/WR F; Bonanos 2007; Ritchie et al. 2010; Clark et al. 2011; Koumpia & Bonanos 2012). Wd1 is therefore expected to have a cool-phase population of single stars or very widely-separated, non-interacting binaries, while binary-mediated evolution in short-period systems is reflected in the very high binary fraction in the Wolf-Rayet population ( $\gtrsim 70\%$ ; Crowther et al. 2006; Clark et al. 2008). This theoretical model is supported by the apparent lack of binaries amongst the population of very luminous mid-B to F hypergiants: to date, the only candidate binary in the cool-phase population is the LBV W243, which has a potential interferometric companion (Mahy et al. 2021), an X-ray excess consistent with the presence of a late-O supergiant (Clark et al. 2019b), and a complex H and He I emission-line spectrum that suggests a hot secondary is ionising the wind of the cool-phase primary (Ritchie et al. 2009b). The presence of high-amplitude pulsational instabilities (Ritchie et al. 2009a; Clark et al. 2010) and the large orbital separation required to accommodate a B–F hypergiant make RV studies of this population extraordinarily challenging, but if any of these cool-phase hypergiants are binary, then they must have such a large separation that the primary can evolve across the Hertzsprung-Russell diagram as an effectively-isolated object, and the most luminous objects in Wd1 are unlikely to be representative of the unevolved binary population in the cluster. In this paper we therefore examine a dataset of more than a hundred O9–B2 stars with masses  $\sim 25\text{--}35M_{\odot}$  (Clark et al. 2020) that are just starting to evolve away from the MS. Unless their initial periods are extremely short, binaries in this population are not expected to have begun to interact (Wellstein et al. 2001), and these systems provide direct insight into the nature of the binary population of Wd1 before the evolutionary pathways for single and multiple stars start to diverge.

Initial results from five epochs of data obtained in 2008 were presented in Ritchie et al. (2009a), hereafter Paper I, which identified two short-period binaries (W43a and W1065) and two candidates (W2a and W232). Further results drawn from a 14-month dataset obtained in 2008–2009 include an orbital solution for the  $23+35M_{\odot}$  double-lined eclipsing binary W13 (Ritchie et al. 2010), and the identification of a 5.05 day orbital period in the X-ray luminous WC9d+O binary W239/WR F (Clark et al. 2011) which likely includes a third massive component responsible for episodic formation of hot dust. The ultimate endpoint of the binary evolution channel are objects like the B1.5 Ia<sup>+</sup>/WNVL hypergiant W5, identified as a potential

remnant of a binary system disrupted by the primary supernova event (Clark et al. 2014), while other papers in this series have focused on complex evolved systems such as the blue stragglers W27 and W30a (O7–8 Ia<sup>+</sup> and O4–5 Ia<sup>+</sup> respectively; Clark et al. 2019a) and the WN9h: binary W44/WR L (Ritchie et al., in prep.). Properties of X-ray bright massive cluster members are discussed by Clark et al. (2019b), hereafter Paper II, and a cluster census, combining the observations discussed here with other archival observations, is presented in Clark et al. (2020), hereafter Paper III.

## 2. Observations & data reduction

**Table 1.** Census of 151 targets included in the FLAMES datasets referenced in this paper, broken down by spectral type from Paper III. The O9–9.5 III category includes objects classified as candidate O binaries based on *I*-band spectral morphology.

Spectral Type	Count
O4–7 Ia <sup>+</sup>	2 <sup>a</sup>
O9–9.5 III / O bin?	50
O9–9.5 I-II	27
B0–B1.5 Ia–Ib	23
B2–B4 Ia	5
B2–B9 Ia <sup>+</sup>	4 <sup>b,c</sup>
A–F Ia <sup>+</sup>	5 <sup>b</sup>
M0–4 Ia	2 <sup>b</sup>
LBV	1 <sup>d</sup>
sgB[e]	1 <sup>e</sup>
Oe / Be	1 <sup>c</sup>
B0.5–1.5 Ia <sup>+</sup> / WNVL	2 <sup>f,g</sup>
WN8–9	2
WN5–7	9
WC8–9	8
Field stars	9*

<sup>a</sup>Clark et al. (2019a), <sup>b</sup>Clark et al. (2010), <sup>c</sup>Paper III, <sup>d</sup>Ritchie et al. (2009b), <sup>e</sup>Clark et al. (2013), <sup>f</sup>Ritchie et al. (2010), <sup>g</sup>Clark et al. (2014). \*One very faint ‘field’ object may be a cluster member, but membership cannot be confirmed.

The VLT/FLAMES survey for massive binaries in Westerlund 1 carried out observations in 2008, 2009, 2011, and 2013, using the FLAMES-GIRAFFE multi-fibre spectrograph on VLT UT2 *Kueyen* with setup HR21 covering the 8484–9001Å range with  $R = \lambda/\Delta\lambda \sim 16200$ . The FLAMES-GIRAFFE pipeline was used to bias subtract, flat-field, and wavelength calibrate the data, while subsequent processing made use of IRAF for the extraction of individual spectra as well as rectification and heliocentric velocity correction. Full details of target selection, fibre prioritisation, and data reduction are given in Paper I, with additional discussion in Paper III. A summary of the full set of targets by spectral type is given in Table 1.

To briefly summarise target selection, the 2008 and 2009 observations focused on four target fields. A *bright* field,

containing 17 spectroscopically-selected targets (14 OB supergiants, two A–F hypergiants, and a WC9d Wolf-Rayet) and five bright photometrically-selected targets<sup>2</sup>, was observed on eleven epochs, while three *faint* fields containing 17 spectroscopically-confirmed cluster members (16 OB supergiants and a WC8 Wolf-Rayet) and 63 photometrically-selected candidates<sup>3</sup> were observed on seven epochs (*faint1*) or six epochs (*faint2*, *faint3*). Observations are summarised in Table 2. A few targets are present in more than one list; duplicates in the *faint* lists were not accounted for in the description of targets in Paper I but have been removed here, leading to slight differences in the number of targets reported. The 2008–2009 dataset was supplemented with additional FLAMES observations obtained in 2011 and 2013, which are summarised in Table 3. Observations in 2011 were primarily focused on two sets of Wolf-Rayet targets (identified as *WN* and *WC* fields), but spare fibres were also allocated to targets of interest in the OB stellar population. 2013 observations focused on three sets of targets, and provided low (*L1...3*) and high (*H1...3*) resolution follow-up observations of objects of interest from the 2008–2009 dataset, along with initial observations of a number of OB targets that had not been observed in previous FLAMES campaigns. The majority of the 2011 and 2013 observations were obtained using setup HR21 and were reduced in the same manner as earlier observations, and only the HR21 setup was used to measure RVs. Observations obtained in other FLAMES modes were used to examine the *R*-band spectra of certain targets; these are described in the text when used.

In addition to the core 2008–2013 dataset, archival observations were used to further investigate a number of targets. Low-resolution FLAMES observations from 2005 focused on a broad set of OB supergiant and late-type targets (labeled as *SG* fields in Table 3), and are described in more detail by Clark et al. (2010). In addition, *R*-band spectra of a number of our targets were acquired in June 2004 using VLT/FORS2 in longslit and mask exchange unit (MXU) modes (Negueruela et al. 2010).

### 3. Analysis

#### 3.1. Radial velocity measurement

RVs were measured by fitting Lorentzian profiles to the strong Paschen series lines in the 8500–9000Å range covered by the FLAMES HR21 setup, using the Levenberg-Marquardt nonlinear least-squares method; example fits to lines with both high and low signal-to-noise ratios (*S/N*) are shown in Figure 1, and summary results for all objects are given in Table 11. Fits were made from  $-500$  to  $+500\text{km s}^{-1}$  relative to the line rest wavelength, which ensures that at low *S/N* the derived RV is not significantly affected by noise or sky residuals overlapping the line core. Exceptions were made in the following cases:

- When fitting the Pa-11  $\lambda 8862$  line in B supergiants the fit was only extended to  $-400\text{km s}^{-1}$  to avoid the influence of the He I  $\lambda 8845$  line bluewards of Pa-11. In very high *S/N* spectra a weak DIB from the C<sub>2</sub> Phillips (2-0)

<sup>2</sup> Identified in Paper I as four O9.5–B0 Iab/b cluster members and one field M2 II/III star.

<sup>3</sup> Identified in Paper III as 55 O9 III–B0 Ia cluster members, one Oe/Be cluster member, and seven field stars.

**Table 2.** Journal of observations during 2008–2009. All observations are in FLAMES HR21 mode.

Date	MJD <sup>a</sup>	$\Delta t^b$	Targets	Int.
20/06/2008	54637.1895	–	Faint 1	3×895s
	54637.2304	–	Faint 2	3×895s
29/06/2008	54646.1846	–	Bright	2×600s
	54646.2239	–	Faint 3	3×895s
18/07/2008	54665.0356	18.85	Bright	2×600s
	54665.0651	18.84	Faint 3	3×895s
	54665.1041	27.87	Faint 2	3×895s
	54665.1439	27.95	Faint 1	3×895s
24/07/2008	54671.1343	6.10	Bright	2×600s
14/08/2008	54692.0423	20.91	Bright	2×600s
	54692.0731	27.01	Faint 3	3×895s
17/08/2008	54695.0941	29.99	Faint 2	3×895s
	54695.1328	29.99	Faint 1	3×895s
04/09/2008	54713.0107	20.97	Bright	2×500s
15/09/2008	54724.0818	11.07	Bright	2×500s
17/09/2008	54726.0148	33.94	Faint 3	3×895s
	54726.0532	30.96	Faint 2	3×895s
19/09/2008	54728.0245	32.89	Faint 1	3×895s
	54728.0554	3.97	Bright	600,700s
25/09/2008	54734.0613	6.01	Bright	2×600s
14/05/2009	54965.1768	231.12	Bright	2×600s
	54965.2061	239.19	Faint 3	3×865s
	54965.2448	239.19	Faint 2	3×865s
	54965.2827	237.26	Faint 1	3×865s
18/05/2009	54969.3198	4.14	Bright	2×600s
	54969.3478	4.07	Faint 1	3×865s
18/08/2009	55061.0310	95.82	Faint 3	3×865s
	55061.0680	95.82	Faint 2	3×865s
20/08/2009	55063.0290	93.68	Faint 1	3×865s
	55063.0575	93.74	Bright	2×600s

<sup>a</sup>The modified Julian day (MJD) is given at the midpoint of integrations.

<sup>b</sup>The time (in days) since the target field was last observed.

system is visible on the blue wing of Pa-11 (see W57a in Figure 1), but does not affect the fit.

- A broad DIB overlaps Pa-13  $\lambda 8665$ , strongly attenuating the blue wing of the line, and the fit was limited to  $\pm 200\text{km s}^{-1}$  from the line centre.

**Table 3.** Journal of supplemental FLAMES observations during 2005, 2011, and 2013. HR21 mode was used unless noted.

Date	MJD <sup>a</sup>	$\Delta t^b$	Targets	Int.
23/03/2005	53454.31865	–	SG <sup>c</sup>	2×877s
	53454.34250	–	SG <sup>d</sup>	2×600s
	53454.35167	–	SG <sup>e</sup>	2×100s
29/05/2005	53519.25658	64.91	SG <sup>d</sup>	2×530s
	53519.26506	64.91	SG <sup>e</sup>	2×100s
13/07/2005	53564.10112	109.78	SG <sup>c</sup>	2×877s
	53564.12375	44.87	SG <sup>d</sup>	2×600s
	53564.13294	44.87	SG <sup>e</sup>	2×100s
17/04/2011	55668.2404	–	WC	3×865s
26/04/2011	55677.2063	–	WN <sup>f</sup>	3×865s
20/05/2011	55701.1855	23.98	WN	3×865s
22/05/2011	55703.1494	34.91	WC	3×865s
24/06/2011	55736.9864	35.80	WN	3×865s
25/06/2011	55737.0293	33.88	WC	3×865s
30/08/2011	55804.0037	–	SG	3×895s
12/04/2013	56394.2703	–	L1 <sup>d</sup>	3×894s
	56394.3156	–	L2 <sup>d</sup>	3×894s
	56394.3598	–	L3 <sup>d</sup>	3×894s
20/05/2013	56432.1406	37.87	L1 <sup>d</sup>	3×894s
10/07/2013	56483.1993	–	H1	3×815s
	56483.2356	–	H2	3×815s
	56483.2713	–	H3	3×815s
21/07/2013	56494.0829	10.88	H1	3×815s
	56494.1207	10.89	H2	3×815s
	56494.1999	10.93	H3	3×815s
23/07/2013	56496.0887	2.01	H1	9×815s
24/07/2013	56497.1969	3.08	H2	3×815s
04/08/2013	56508.1094	13.91	H3	3×815s
	56508.1730	12.08	H1	3×815s
07/08/2013	56511.1590	13.97	H2	2×815s
08/08/2013	56512.2129	1.05	H2	3×815s

<sup>a</sup>The modified Julian day (MJD) is given at the midpoint of integrations.

<sup>b</sup>The time (in days) since the target field was last observed.

<sup>c</sup>LR4 mode.

<sup>d</sup>LR6 mode.

<sup>e</sup>LR8 mode.

<sup>f</sup>HR16 mode.

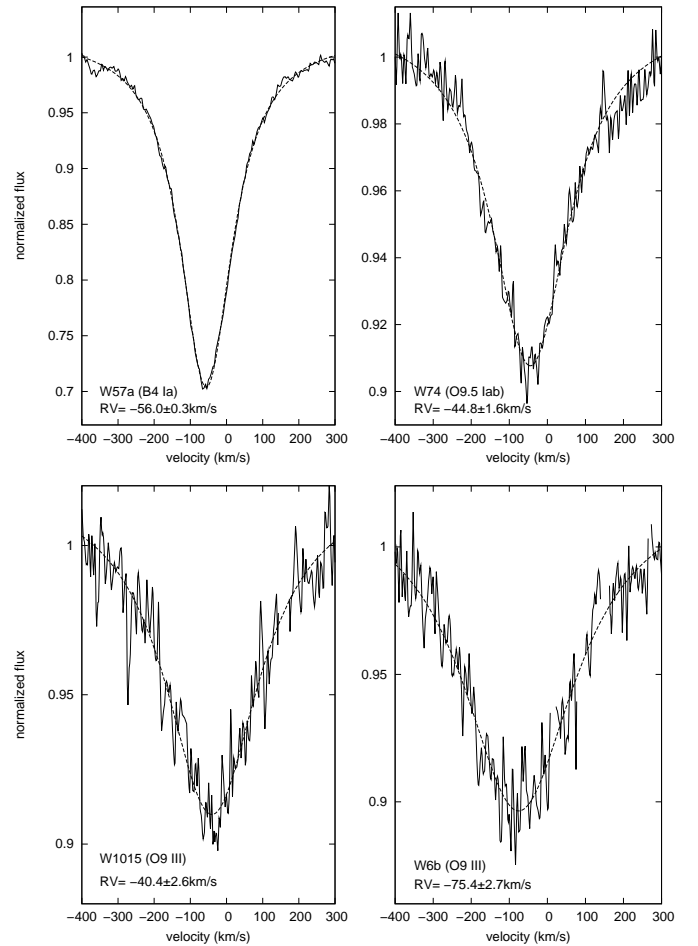


**Fig. 1.** Example fits to the Pa-11 line at a variety of  $S/N$  representative of the targets included in this programme. Note that W6b is a single-lined binary.

– In very broad-lined O-type stars the line width can exceed  $\pm 500 \text{ km s}^{-1}$ , and the fitting region was extended to fully accommodate the line profile.

In a number of cases, targets were included in more than one target list and were observed twice (e.g. W55, W71, or W1036), or even three times (W232, W1065) on the same night. In all but one case measured RVs are in agreement to within the respective fitting errors, and typically agree to within  $\sim 1 \text{ km s}^{-1}$ , suggesting that our RV measurements are not significantly affected by transient noise or sky residuals; W232 is the sole exception, and is discussed further in Section 5.2. A strong, well-defined DIB at  $8620 \text{ \AA}$  (Damineli et al. 2016) serves as a check for zero-point errors in the wavelength calibration of individual spectra.

While the Pa-12  $\lambda 8750$  line was included in the analysis in Paper I, subsequent examination of the effect of the C<sub>2</sub> Phillips (2–0) band system on the redwards flank of the line has led to this line being excluded from this analysis, as these interstellar features lead to a broadening and systematic shift redwards by  $\sim 10 \text{ km s}^{-1}$  relative to Pa-11 and Pa-13 (see also discussion in Ritchie et al. 2010). While the increased fitting error caused by the asymmetric Pa-12 line profile reduces the impact of this offset in the RVs reported in Paper I, we find an improved RV measurement if the line is omitted completely, and in early B objects Pa-11 and Pa-

13...15 in are excellent agreement. In high  $S/N$  spectra a bluewards shift in the Pa-16  $\lambda 8502$  line from blending with C III  $\lambda 8500$  can be seen in objects as late as B0.5–1 Ia, and this line is also consequently excluded. However, most of the targets considered in this paper come from a population of lower-luminosity stars with spectral types earlier than B0. The higher Paschen series lines are fading rapidly in these objects, and RVs were measured using the Pa-11 and Pa-13 lines alone. The decreasing  $S/N$ , weakening line strength, and increasing line width towards lower luminosity classes leads to a systematic increase in RV measurement errors towards earlier spectral types: while errors internal to the Levenberg-Marquardt fit are generally below  $1\text{ km s}^{-1}$  for all Paschen lines in the most luminous objects in our target list, which have  $S/N > 100$ , at O9.5 II mean fitting errors are generally around  $3\text{ km s}^{-1}$  for Pa-11 and  $\gg 5\text{ km s}^{-1}$  for Pa-13 and Pa-14, leading to an error-weighted RV dominated by the measurement of Pa-11. We also note that a subset of faint objects (with  $I \geq 14.5$ ) have very broad, weak Paschen series lines and significantly higher fitting errors; these were proposed as heavily-blended SB2s in Paper III, and we briefly return to these objects in Section 6.2.

### 3.2. Sky emission lines

Sky emission lines that are not fully removed by sky spectra subtraction are often problematic, especially for the lower-luminosity targets in our dataset. In the majority of cases these lines do not fall near the Paschen series absorption lines used for RV measurement, but when these features overlap the resultant fit may be a poor match to the line core: an example is shown in the left panel of Figure 2, with a strong sky residual reaching  $\sim 20\%$  above the continuum level falling  $\sim 40\text{ km s}^{-1}$  bluewards of the line centre. Such features are easily identified as a significant departure from the local moving average, and we take the deliberately simplistic approach of locating the peak of the sky emission line and excluding the five data bins on either side, with testing showing that more complex removal does not result in appreciable improvement. The right panel of Figure 2 shows the improved fit after sky line removal.

### 3.3. Binary candidate identification

As discussed in Paper I, RV variability is not necessarily orbital, and may also result from wind effects and radial and/or non-radial pulsations (see also Sana et al. 2013 and Lohr et al. in prep.). Taking the LBV W243 (A3 Ia<sup>+</sup>) as an example of a high-amplitude pulsator, 20 epochs of data display RVs spanning  $\sim 24\text{ km s}^{-1}$  with variability of  $\sim 1\text{--}2\text{ km s}^{-1}$  on a timescale of days (individual fitting errors  $< 1\text{ km s}^{-1}$ ). No periodicity is apparent, and the sheer size of W243 ( $R_* \sim 420R_\odot$ ; Ritchie et al. 2009b) precludes a binary interpretation for the rapid RV variability we observe. Luminous B supergiants and A–F hypergiants display variability of similar magnitude and cadence (Clark et al. 2010). We therefore follow Sana et al. (2013) and examine the maximum significance of RV differences between any two epochs of observation

$$\sigma_{\text{det}} = \max \left( \frac{|v_i - v_j|}{\sqrt{\sigma_i^2 + \sigma_j^2}} \right) \quad (1)$$

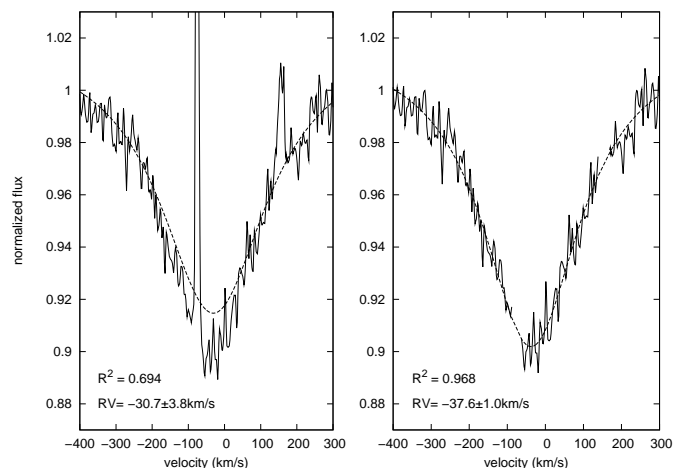


**Fig. 2.** Effect of unsubtracted sky lines on RV determination. (*Left Panel*) Pa-11 line profile for W17 (20/06/2008) with unsubtracted lines at  $-75\text{ km s}^{-1}$  and  $+160\text{ km s}^{-1}$ . (*Right Panel*) the same Pa-11 line after the sky lines were removed. In each panel, the RV and goodness-of-fit metric  $R^2$  derived from the Levenberg-Marquardt method are listed, demonstrating the reduced error and improved fit following sky line removal.

and require that at least one pair of observations display  $\Delta\text{RV} = |v_i - v_j|$  that exceeds a minimum amplitude threshold  $C$ . As apparently non-orbital variability in measured RVs can exceed  $\sim 20\text{ km s}^{-1}$  in the luminous evolved population of early–mid B supergiants in Wd1, we adopt  $C > 25\text{ km s}^{-1}$  and  $\sigma_{\text{det}} > 4$  as indicative of a likely binary nature: failure to meet this clip level does not preclude binarity, but means that we cannot separate orbital motion from other effects with the available data. The classification of targets as spectroscopic binaries is clearly dependent on the choice of velocity cut, and Figure 3 shows the fraction of objects selected as candidate binaries or pulsational variables as the cut-off velocity is increased. A break in the distribution is seen at  $\sim 28\text{ km s}^{-1}$ , suggesting that this may mark the maximum amplitude of wind and/or pulsational effects. This is in good agreement with the  $25\text{--}30\text{ km s}^{-1}$  threshold for OB supergiants suggested by Simón-Díaz et al. (2020). Although this is slightly above our adopted  $25\text{ km s}^{-1}$  threshold, potential photospheric variability in this range is limited to a few highly-luminous B supergiants and increasing the threshold further would start to eliminate a number of systems that are clearly *bona fide* binaries. A simple extrapolation of the slope above  $\sim 40\text{ km s}^{-1}$  towards lower RVs would suggest that roughly  $\sim 10\%$  of our total targets may be low-amplitude binaries that cannot be distinguished from a larger population of pulsational variables. We return to this topic in Section 10.

### 3.4. Period search

To search for periodicities in the RV data of binary candidates, we first compute the Lomb-Scargle periodogram (Lomb 1976; Scargle 1982): an example is shown in Figure 4. We take 250 days as the upper limit for the search, and use the target’s spectral type as a guide to the lower limit, adopting 1 day for O9 III, 2 days for O9–9.5 I–II,

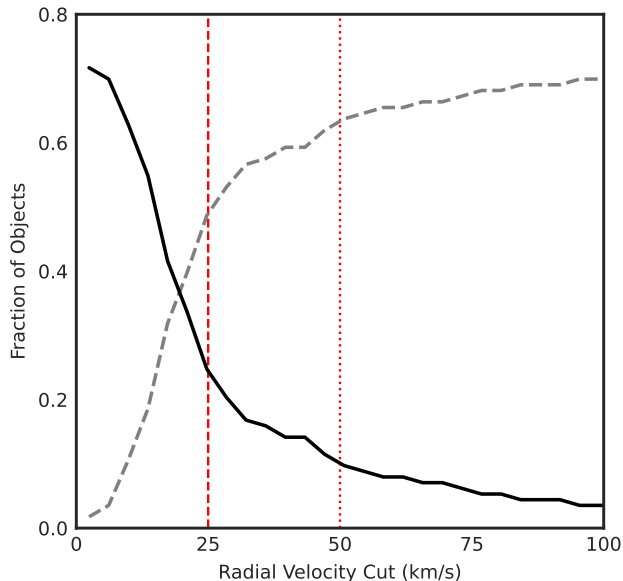


**Fig. 3.** Fraction of systems passing a RV cut at  $C$  km s<sup>-1</sup> to separate binaries from pulsational variables. The solid line marks the fraction identified as binaries ( $\Delta RV > C$ ), while the dashed line identifies the fraction identified as variables ( $\Delta RV < C$ ). The vertical lines mark the 25 km s<sup>-1</sup> (dashes) and 50 km s<sup>-1</sup> (dots) thresholds discussed in the text.

3 days for B0–B1.5 Ia, and ten days for objects of spectral type B2–4 Ia; in each case, we consider shorter periods to be unphysical, as they require an orbital separation incompatible with the spatial extent of a (non-interacting) primary (cf. Martins et al. 2005). We then carry out a string-length minimisation search (Dworetzky 1983) to confirm any identified period. If the two methods are in agreement, the final determination of the orbital period is carried out using the Liège Orbital Solution Package<sup>4</sup> (hereafter LOSP), with non-zero eccentricity permitted. We regard an orbital period as secure if:

1. The strongest peak in the Lomb-Scargle periodogram has a Baluev (2008) false alarm probability  $< 1\%$ .
2. The periodogram, string-length search, and LOSP period search identify the same orbital period.
3. No alternative periods with similar peak strengths exist.

If the false alarm probability is in the range 1 – 5% then we refer to the solution as a *candidate* period provided that the other conditions are met. In some cases we discuss possible orbital periods that do not meet these criteria, noting that these *tentative* identifications must be confirmed with future observations.

### 3.5. Orbital parameters

The systemic velocity  $\gamma$ , semi-amplitude  $K$ , eccentricity  $e$ , and longitude of periastron  $\omega$  were determined using LOSP, fixing the orbital period  $P$  at the value determined by the period search discussed in Section 3.4. As an independent

<sup>4</sup> <https://stsci.edu/~hsana/losp.html>

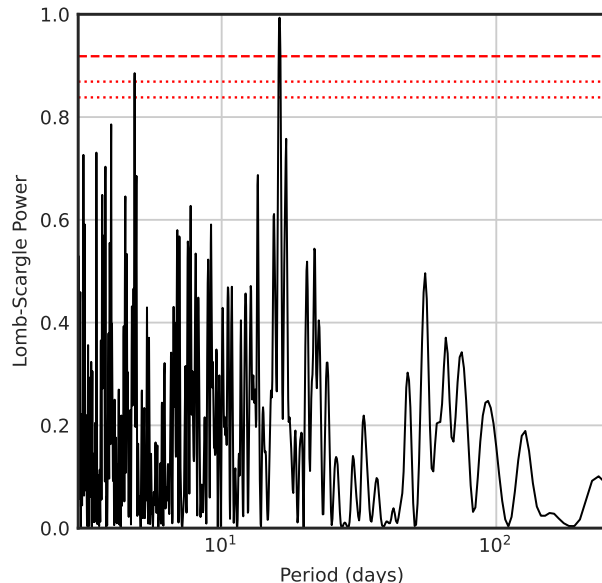


**Fig. 4.** Lomb-Scargle Periodogram for W43a. Horizontal lines mark (from top to bottom) Baluev (2008) 1%, 5%, and 10% false alarm probabilities. The strongest peak is at 16.241 days, and the minimum string length (not shown) occurs at 16.243 days.

check, we then repeated the analysis using THE JOKER (Price-Whelan et al. 2017), a custom Monte Carlo sampler for sparse RV datasets: in all cases, the two methods produced orbital solutions that were in agreement to within their respective errors. Orbital solutions from LOSP are discussed in Section 5 and summarised in Table 5.

We note that many objects only have limited sampling, and in the majority of cases orbital solutions should be regarded as provisional: for this reason, we do not attempt more detailed analysis of aggregate parameters at this time (e.g. the distribution of orbital eccentricities). In particular, poor sampling of the extremes of the RV curve or (in eccentric systems) the periastron passage may lead to significant inaccuracies in orbital parameters. Comparison of our results with an initial analysis based on the 2008–2009 dataset alone suggests that additional data do not *substantially* affect our conclusions; further observations have not ruled out any targets that were identified as short-period binaries in the initial analysis. However, additional data often led to small changes in the determinations of semi-amplitude, period, and eccentricity, and we expect that future observations will continue to refine the results presented here.

## 4. Binary Identification

Of the 151 objects listed in Table 1, 6 are cluster members with only a single epoch of observation, and 8 are field stars. A 2.26 day eclipsing binary<sup>5</sup> reported by Bonanos (2007) is tentatively identified as a cluster member based on the strength of the 8620 Å DIB, but cluster membership cannot be confirmed: this object is extremely faint ( $I = 16.2$ )

<sup>5</sup> Located near the core of the cluster at J16:47:05.79 -45:51:33.3

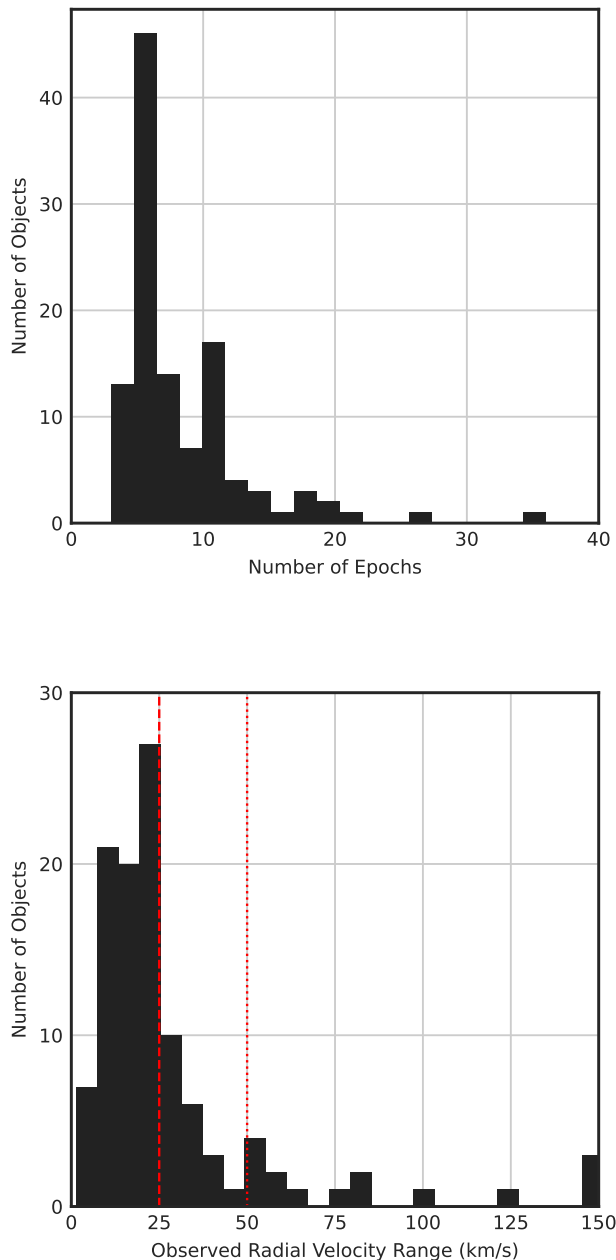


**Fig. 5.** (*Top Panel*) Number of epochs for each object, (*Bottom Panel*) Distribution of observed RV ranges, with vertical lines marking the  $25\text{km s}^{-1}$  and  $50\text{km s}^{-1}$  cuts.

and cannot be analysed further. In addition, W9 (sgB[e]; Clark et al. 2013) and W1004 (Oe/Be; Paper III) show emission-line spectra devoid of photospheric absorption features suitable for RV measurement, while 21 Wolf-Rayet targets are discussed separately in Section 7. We therefore examine a population of 113 O–M stars, of which 105 are OB stars: histograms of the number of epochs of observation and the RV ranges observed are shown in Figure 5, while full results from this RV analysis are shown in Figure 6.

We find that 34 targets (30% of the sample of 113 objects) do not display statistically-significant RV changes<sup>6</sup>. Almost all are O-type stars from luminosity class Ib–III, with correspondingly reduced  $S/N$  and increased fitting error, and many have limited sampling, implying that we may not be observing the full RV range. Four objects fail the statistical-significance test despite exceeding the  $\Delta RV > 25\text{km s}^{-1}$  threshold. Three are faint, very broad-lined stars with large measurement errors, while the fourth is an O9.5 Iab star with only three epochs of observation; in each case we also find  $\sigma_{\text{det}} < 4$ . Only one B-type star (W1009; B0 Ib) does not display statistically-significant RV variability.

Of the remaining 79 targets, 43 (or 38% of the sample) do not meet the dual requirements of Section 3.3: in all but one case we find  $\sigma_{\text{det}} > 4$  but  $\Delta RV < 25\text{km s}^{-1}$ , while one object meets neither requirement. These targets are predominantly B0 Ib or later, with the increased luminosity, narrow Paschen series lines, and apparently-ubiquitous presence of photospheric pulsations in B-type supergiants leading to increased detection significance ( $\sigma_{\text{det}}$ ), although some O-type stars of luminosity class I or II also fall into this group. While these objects cannot be classified as spectroscopic binaries based on their RV variability, we note that one object in this group (W23a; B2 Ia) displays a composite spectrum that confirms its binary nature; it is discussed further in Section 5.8.

Finally, 37 targets (or 32% of the sample) fully satisfy the criteria for binary classification. Most interesting are the 23 objects with  $\sigma_{\text{det}} > 15$  or  $\Delta RV > 50\text{km s}^{-1}$ : these targets offer high  $S/N$  or large changes in RV, making them suitable for more detailed analysis in Section 5. We note that these selection criteria favour the narrow line widths and high luminosity (and hence high  $S/N$ ) of B supergiants, although these selection criteria are again also met by a number of O9.5 II stars, as well a few targets from earlier spectral types that have large RV amplitudes. In general, less can be said about the 14 objects that pass our selection criteria but lie in the range  $25 < \Delta RV < 50\text{km s}^{-1}$  and  $5 < \sigma_{\text{det}} < 15$ . Two examples (W30a and W1030) have very strong secondary indicators of binarity and an extensive baseline of observations that permit further analysis; these two objects are also discussed in Section 5. The remaining 12 objects are all O-type stars, with only one classified as a supergiant, and display low semi-amplitudes, broad lines, and low  $S/N$ : with fewer than ten epochs of observation, it is impossible to select between candidate orbital solutions with any confidence. Therefore, while it is possible to identify statistically-significant RV changes in early-type objects, along with supporting evidence for binarity based on the  $R$ - and  $I$ -band spectral morphology (see also Paper III), it is usually not possible to analyse the low-luminosity O9 III population in detail: we discuss these systems further in Section 6.

#### 4.1. Average cluster radial velocity

We determine the cluster systemic velocity from the error-weighted average of the RVs of 58 OB stars in our survey that have  $\Delta RV < 25\text{km s}^{-1}$  and more than five epochs of

<sup>6</sup> RV variability is considered statistically-significant if we can reject the null hypothesis that no RV changes are present at the 99.99% confidence level.

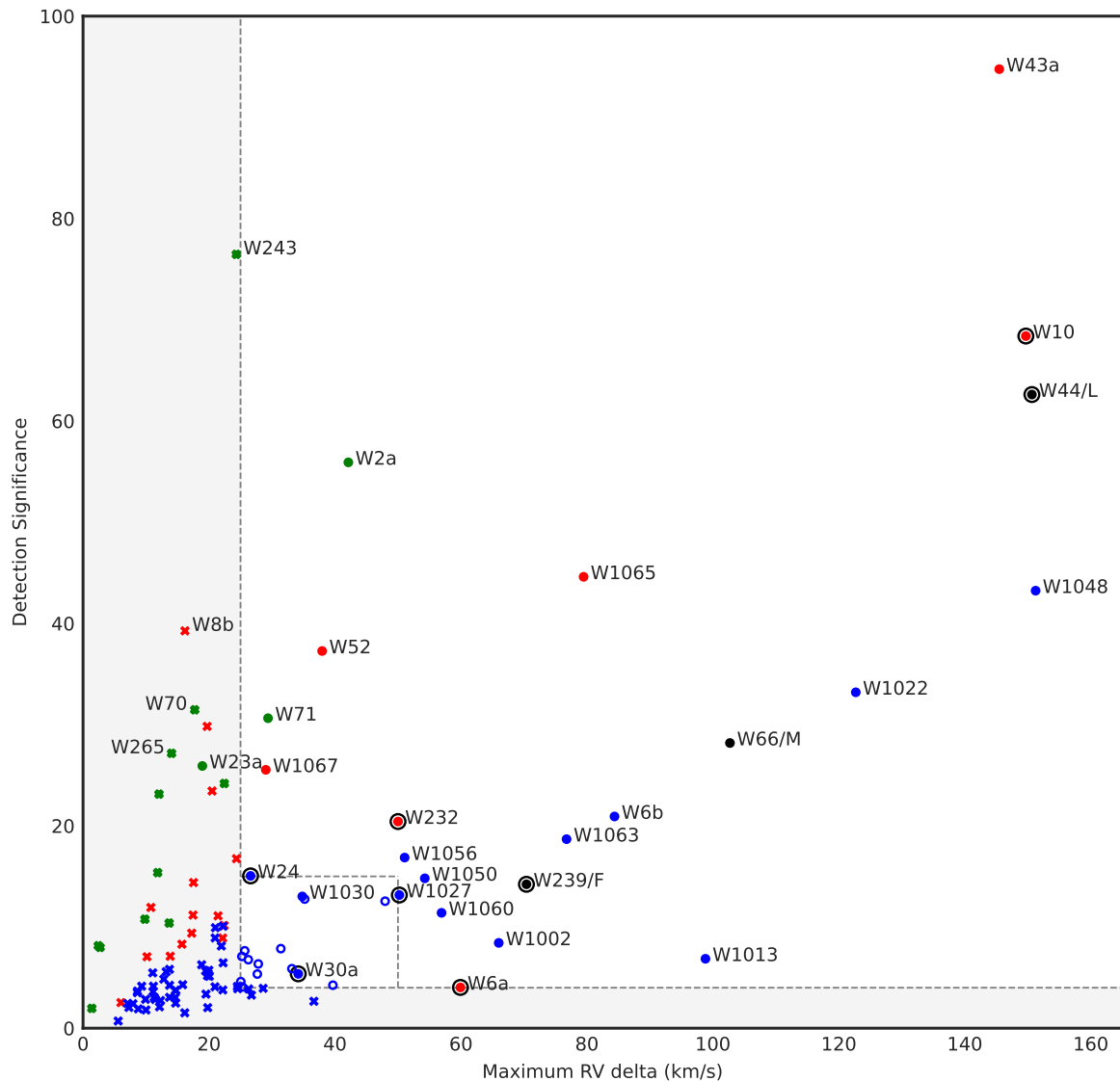


**Fig. 6.**  $\Delta RV$  vs.  $\sigma_{\text{det}}$ . Filled circles represent binaries, open circles represent *candidate* binaries, and crosses represent systems that do not meet the dual criteria described in Section 3.3. Wolf-Rayet stars are marked in black, O-type stars in blue, B0-B1.5 stars in red, and later types are in green. X-ray detections from Paper II are marked with a black circle. Dashed lines and shaded areas mark the cutoffs described in the text. Note that W13, W36, W53a, and W1021 have RV ranges that lie outside the bounds of this figure.

observation, with the latter criterion ensuring that time-averaging limits any extremes of pulsational variability. The absorption lines used for RV measurement are expected to form quite close to the photosphere and therefore no RV offset due to wind-filling is expected, implying that measured RVs should be consistent across this population. The resulting cluster RV of  $-43.1 \text{ km s}^{-1}$  is in good agreement with the mean RV of  $-44.7 \pm 1.9 \text{ km s}^{-1}$  found from interstellar

$C_2$  Phillips (2-0) absorption features in the spectra of the luminous B2–4 Ia supergiants W57a, W70, and W71, suggesting the absorbing material is likely local to the cluster. It is also in agreement with the time-averaged *Gaia* EDR2 RVs for the cool hypergiants W4, W8a, W26 and W265, implying no substantial systematic effects are present in our observations. Detailed analysis of the cluster RV and



its implications for the distance and location of Wd1 will be presented in Negueruela et al. (in prep.).

## 5. Binaries

**Table 4.** The 26 targets discussed in Section 5. The three objects listed as *Morphology* or *X-Ray* do not meet the criteria defined in Section 3.3, but have spectra or X-ray luminosities that unambiguously indicate a binary nature.

Type	Count	New?	Identification
Eclipsing SB2	2	0	W36 <sup>a</sup> , W1021 <sup>a</sup>
SB2	2	1	W10 <sup>b</sup> , W53a
B0–B2.5 Ia	8	6	W2a, W6a, W43a <sup>c</sup> , W52, W71, W232, W1065 <sup>c</sup> , W1067
O9–9.5 Iab–Ib	3	3	W24, W1027, W1048
O9–9.5 II–III	6	6	W6b, W1022, W1050, W1056, W1060, W1063
O + O	2	2	W1002, W1013
Morphology	2	2	W23a, W1030
X-Ray	1	0	W30a <sup>d</sup>
Total	26	20	

Previously confirmed as binary in: <sup>a</sup>Bonanos (2007), <sup>b</sup>Negueruela et al. (2010), <sup>c</sup>Ritchie et al. (2011), <sup>d</sup>Clark et al. (2019a).

Table 4 lists the objects considered in this section. Of the 23 OB stars with high detection significance ( $\sigma_{\text{det}}$ ) and/or large RV amplitudes, W36 and W1021 are eclipsing SB2s first reported by Bonanos (2007), W10 was identified as a SB2 by Negueruela et al. (2010), and W43a and W1065 were identified as SB1s by Ritchie et al. (2011). Of the remainder, six are B0–B2.5 Ia stars, while twelve (including one newly-identified SB2) are O-type stars. In addition, we include three objects that do not meet the criteria in Section 3.3 but are unambiguously binary based on secondary indicators: W23a (B2 Ia) and W1030 (O9.5 Ib) have spectra that are inconsistent with a single spectral type, while the high X-ray luminosity of the blue straggler W30a (O4–6 Ia<sup>+</sup>) implies it is a colliding-wind binary.

### 5.1. W10

W10 was noted as a SB2 (B0.5 I + OB) by Negueruela et al. (2010), based on VLT/FORS observations that showed broad H $\alpha$  emission and double-lined He I $\lambda$ 6678,7065. It is also detected at X-ray (Clark et al. 2008) and radio (Andrews et al. 2019) wavelengths. We observed W10 on four nights in 2011 and a further four nights in 2013, with the dataset comprising one spectrum in HR16 mode (showing a single He I $\lambda$ 7065 line) and ten spectra in HR21 mode. Although W10 appears single-lined in most observations, with RVs in the range  $-50 \text{ km s}^{-1}$  to  $-65 \text{ km s}^{-1}$ , on MJD 56483.20 the Paschen series lines are clearly double, with the more luminous primary at

$+83 \pm 2 \text{ km s}^{-1}$  and a weaker secondary at  $-164 \pm 6 \text{ km s}^{-1}$  (see also Figure 1 in Paper II).

These observations suggest the system has a high eccentricity, with the B0.5 I primary dominating the composite spectrum in most epochs and the secondary only visible near periastron. Such a configuration is also required to understand the X-ray properties of the system: W10 appears softer and less X-ray luminous than other SB2s in Wd1, possibly reflecting observations at a phase where the wind collision zone was weak or obscured. Unfortunately, any orbital fit is strongly driven by the single epoch of observation near periastron, and we cannot distinguish between a number of potential periods in the range  $\sim 5 - 20$  days. W10 appears single-lined on MJD 56494.08, implying a rapid periastron passage, but further observations near periastron are required to securely determine orbital parameters. However, we can estimate a mass ratio of  $\sim 0.90 \pm 0.05$ , and we tentatively classify the secondary as  $\sim$ O9.5 II based on the relative strength of the Pa-11 lines. The presence of a weak He I $\lambda$ 8845 absorption line confirms a  $\sim$ B0.5 Ia classification for the primary.

### 5.2. The peculiar B0 Iab star W232

W232 (=C07-X6; Clark et al. 2008) was identified as probable binary in Paper I<sup>7</sup>, based on the presence of significant RV changes on short timescales. It was classified as B0 Iab based on its *R*-band spectrum (Negueruela et al. 2010), although the higher Paschen series lines suggest a slightly earlier  $\sim$ O9.5 Ib spectral type may be appropriate. W232 was included on the *bright*, *faint1*, and *faint2* target lists, and we obtained 24 RV measurements in 2008–2009, along with a further 12 RV measurements in 2013. In a number of cases multiple observations were obtained on the same night, with low-level line profile variability leading to differences in measured line centres of up to  $5 \text{ km s}^{-1}$  in consecutive spectra: this is unlike other objects that were observed repeatedly on the same night, such as W71 and W1065, where consecutive spectra are in excellent agreement.

The Lomb-Scargle periodogram shown in Figure 7 reveals two strong periodicities at 0.9067 days and 9.980 days, which remain consistent across the 2008–2009 and 2013 datasets. The former appears inconsistent with an orbital interpretation, with the expected radius of a B0 Iab primary (Martins et al. 2005) implying that any companion would be almost engulfed. However, W232 appears very similar to other O9.5–B0 supergiants in Wd1, and does not display the complex, blended, and time-varying spectra seen in very short period interacting systems such as W6a or W53a. Nevertheless, if the photometry of Bonanos (2007) is folded onto a 0.9067 day period then a clear low-level sinusoidal variation is apparent (see the lower panel of Figure 7), suggesting this periodicity is not spurious, and its persistence from photometry obtained in 2006 to RV data obtained in 2008–2009 and 2013 implies that the underlying process is stable and therefore unlikely to represent a transient or quasi-periodic photospheric process. The alternative periodicity provides an orbital solution with  $P = 9.9778 \pm 0.0009$  days,  $K_1 = 14.7 \pm 2.0 \text{ km s}^{-1}$ ,  $\gamma = -45.3 \pm 1.5 \text{ km s}^{-1}$ ,  $e = 0.41 \pm 0.06$ , and  $\omega = 256 \pm 42$  degrees. Scatter around the best-fit solution is present, re-

<sup>7</sup> Note that W232 was incorrectly identified as W234 in Paper I.

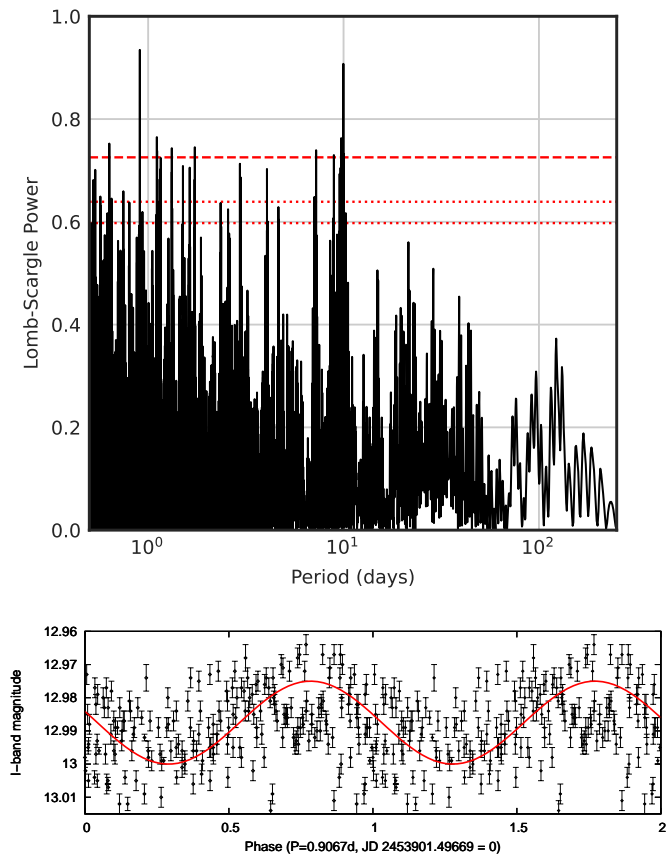


**Fig. 7.** (Top) Lomb-Scargle Periodogram for W232, showing strong peaks in the RV data at 0.9067 days and 9.980 days. (Bottom) Photometry from Bonanos (2007) folded on to the 0.9067 day period. The line marks the best-fit sinusoid.

flecting rapid line-profile variability superimposed on orbital modulation.

W232 is somewhat more X-ray luminous than expected for an isolated star (Clark et al. 2008), suggesting a binary interpretation is appropriate, and we note that the sgB[e] binary GG Carinae also displays stable photometric and RV variability on a period of  $\sim 1.53$  days that is well below its  $\sim 31$  day orbital period (Porter et al. 2021). GG Car has a significantly eccentric orbit, and these short-period pulsations result from tidally-driven oscillations at the  $l = 2$   $f$ -mode frequency, with the largest variability occurring at periastron. In the case of W232, we note that there is an exact integer ratio between the two identified periods, suggesting the 0.9067 day period is a tidally excited oscillation in a  $g$ -mode of the primary that arises from a resonance between an orbital harmonic and a mode frequency (Willems & Aerts 2002). This tidal resonance would explain both the long-term stability of the 0.9067 day oscillation and the rapid line profile variability, which may arise from higher order  $g$ -modes. The combination of significant eccentricity, short period, and tidally-excited oscillations suggest that W232 may therefore be an example of a massive ‘heartbeat star’ (Fuller 2017); if confirmed, it would represent one of the most massive examples known.

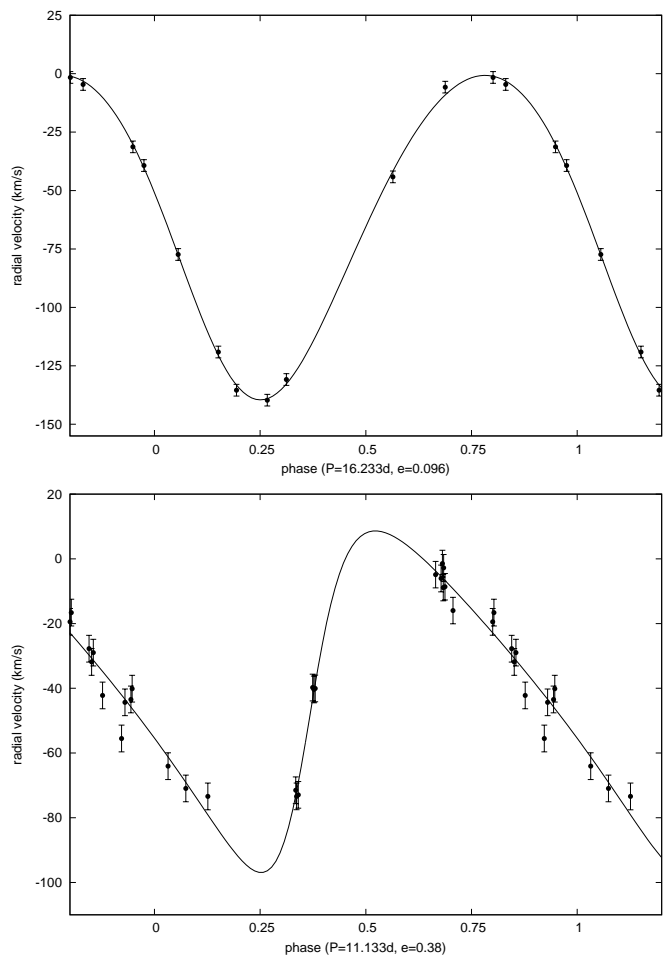


**Fig. 8.** RV curve for the B0 supergiants W43a (Top Panel) and W1065 (Bottom Panel).

### 5.3. Early-B supergiant SB1s: W43a, W52, W1065, and W1067

W43a is a B0 Ia supergiant that was identified as an SB1 displaying low-level pulsational variability in Paper I (see also Ritchie et al. 2011). We find a period  $16.2333 \pm 0.0048$  days, with  $K_1 = 69.4 \pm 0.9$  km s $^{-1}$  and  $\gamma = -64.4 \pm 0.8$  km s $^{-1}$ , while the orbit appears slightly eccentric, with  $e = 0.096 \pm 0.017$  and  $\omega = 149 \pm 9$  degrees. The RV curve is plotted in Figure 8. No eclipses are seen in the photometry of Bonanos (2007), but complete phase coverage is not available and an eclipsing system cannot be ruled out.

W1065 (B0 Ib; previously identified as W3003) was also identified as a short-period binary in Paper I. It was included in the 2008–2009 *bright*, *faint2* and *faint3* fields, giving a total of 23 observations, while four additional observations were obtained in 2013. The orbital period is  $11.1330 \pm 0.0012$  days, with  $e = 0.38 \pm 0.05$ ,  $\omega = 256 \pm 13$  degrees,  $\gamma = -39.4 \pm 2.6$  km s $^{-1}$ , and  $K_1 = 52.8 \pm 3.6$  km s $^{-1}$ . The semi-amplitude implies a lower inclination and/or lower-mass secondary than W43a. The RV curve is again plotted in Figure 8. W1067 (B0 Ib; previously identified as W3004) appears very similar to W1065. It was duplicated on the *bright* and *faint2* lists, providing 17 observations in 2008–2009, and we find a  $6.125 \pm 0.021$  day period

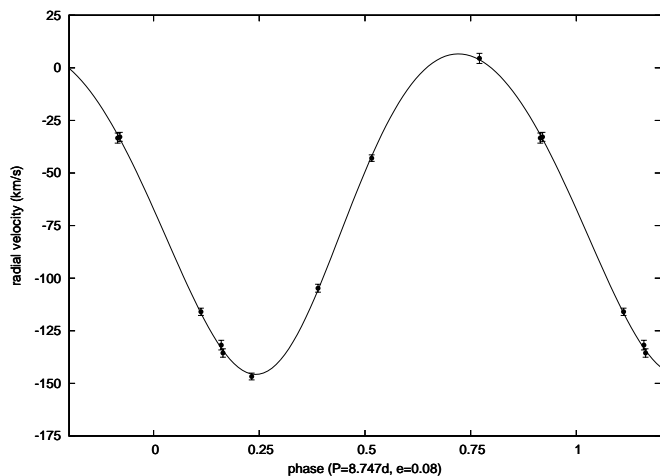


**Fig. 9.** RV curve for the O9.5 Ib supergiant W1048.

with  $K_1 = 13.2 \pm 3.8 \text{ km s}^{-1}$  and  $\gamma = -47.0 \pm 0.9 \text{ km s}^{-1}$ . As with W1065, the best-fit solution is eccentric, with  $e = 0.52 \pm 0.16$  and  $\omega = 355 \pm 15$  degrees. Two low-resolution  $R$ -band spectra from 2013 are available, and we note  $\text{H}\alpha$  in emission with a weak P Cygni profile superimposed on a broader base, which is inconsistent with an isolated B0 Ib star (Negueruela et al. 2010). He I absorption features appear single lined.

Finally, W52 (B1.5 Ia) was only observed on five nights in 2013, but RVs obtained on consecutive nights (MJD=56511.2 and 56512.2) confirm that W52 is a short-period binary. There is insufficient data for a satisfactory period search, but Bonanos (2007) finds W52 to be a 6.7 day periodic variable, and we tentatively identify a  $6.624 \pm 0.108$  day period, with a semi-amplitude of  $\sim 25 \text{ km s}^{-1}$  and an apparently-circular orbit. The RV curve is not well sampled, but the close correspondence between the tentative RV solution and the photometric modulation suggests that the correct orbital period may have been identified. Additional observations are required to determine a robust solution.

None of these four systems are detected at X-ray wavelengths (Clark et al. 2008), and none display any spectroscopic features attributable to a secondary, which are likely OB III-V objects with a lower luminosity and weaker wind than their early-B supergiant primaries.

#### 5.4. W1048

W1048 was identified as a periodic variable by Bonanos (2007). Nine observations were obtained with FLAMES in 2013, including observations on consecutive nights, and the system displays large RV changes that confirm its binary nature. It was not possible to reconcile the RV data with a 5.2 day periodicity reported by Bonanos (2007), and we instead find an orbital period of  $8.747 \pm 0.021$  days with  $K_1 = 76.2 \pm 1.0 \text{ km s}^{-1}$  and  $\gamma = -64.0 \pm 0.6 \text{ km s}^{-1}$ . Like W43a, the system appears slightly eccentric, with  $e = 0.08 \pm 0.03$  and  $\gamma = 205 \pm 8$  degrees. The RV curve is shown in Figure 9. Paper III classifies W1048 as B1.5 Ia, but this appears erroneous: W1048 displays a slightly earlier spectrum than W1065 (B0 Ib) and is reclassified as O9.5 Ib accordingly.

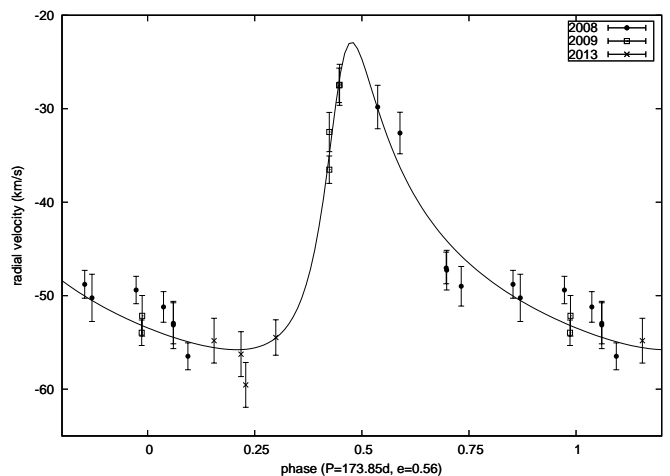


**Fig. 10.** RV curve for the 174 day O9.5 Ib binary W1030. Observations from 2008 (filled circles), 2009 (open squares), and 2013 ( $\times$  symbols) are indicated.

Like the early-B supergiants discussed in Section 5.3, W1048 is not detected at X-ray wavelengths (Paper II), but the large semi-amplitude implies a massive secondary at favourable inclination. No archival observations are available, precluding a broader search for features attributable to the secondary, but refolding the  $I$ -band photometric observations of Bonanos (2007) onto our 8.747 day period suggests that a shallow  $\sim 0.1$ -magnitude eclipse may be present, with a near-contact configuration. The photometric data have considerable scatter and are not suitable for detailed modelling, but a further programme of spectroscopic and photometric observations of W1048 would place constraints on the mass of objects entering the supergiant phase.

#### 5.5. W1030

W1030 (O9.5 Ib; previously named W3005 in Paper I) is located  $\sim 2'$  south of the cluster core, corresponding to a projected distance  $\sim 3 \text{ pc}$  at a distance of 5 kpc. It was duplicated on the 2008–2009 *bright* and *faint1* lists and was observed 18 times in that period. Four additional spectra were obtained in 2013.  $R$ -band spectra show infilled  $\text{H}\alpha$ , while in the  $I$ -band C III  $\lambda 8500$  appears unexpectedly weak for an O9.5 supergiant and it also appears too luminous for its O9.5 Ib classification. W1030 may be a  $\sim \text{B0 Ia}$  star with a spectrum diluted by a  $\sim \text{O9.5 II}$  companion, although no direct evidence for the secondary is observed.

RVs obtained in 2008 show a steady increase from  $-30 \text{ km s}^{-1}$  to  $-56 \text{ km s}^{-1}$ , with lack of any significant excursions on timescales of days–weeks precluding a short orbital period. We find an orbital period of  $173.85 \pm 0.72$  days, by far the longest period currently identified in Wd1, with  $K_1 = 16.5 \pm 1.4 \text{ km s}^{-1}$  and  $\gamma = -46.6 \pm 0.6 \text{ km s}^{-1}$ . The orbit is eccentric, with  $e = 0.56 \pm 0.05$  and  $\omega = 322 \pm 7$  degrees, and the periastron passage is fortuitously well sampled by the 2008 and 2009 observations.

### 5.6. O9.5 II SB1s: W1022, W1050, W1056, and W1060

W1022, W1050, W1056, and W1060 are four very similar systems, with spectra close to W86 (O9.5 Ib) but with broader wings to the Paschen series lines and somewhat lower  $I$ -band magnitudes, leading to an O9.5 II classification. Low-resolution FORS2/MXU spectra are available for W1022 and W1050, with both objects appearing single-lined with  $H\alpha$  in absorption (see Figure 6 in Paper III). A low-resolution LR6-mode FLAMES spectrum of W1056 shows narrow  $H\alpha$  and [N II] nebular emission lines superimposed on a broad, possibly partially-infilled, photospheric  $H\alpha$  absorption line, and we note that W1056 is detected in ATCA observations by Andrews et al. (2019). No additional spectroscopy exists for W1060. All four objects were observed in the 2008–2009 and 2013 campaigns, providing a five-year baseline with either ten or eleven observations. All display  $\Delta RV > 50 \text{ km s}^{-1}$ , confirming them as binaries, although period determination is harder: only one object has a Baluev (2008) false alarm probability below 1%, with the other three objects only having *candidate* periods. None are reported as X-ray detections in Paper II.

W1022 shows some of the largest RV changes in our sample, with  $\Delta RV > 120 \text{ km s}^{-1}$  and a delta of more than  $50 \text{ km s}^{-1}$  in the space of two nights that confirms a short-period system. Somewhat surprisingly, the orbital solution is not very well constrained. We find a candidate period of  $6.175 \pm 0.004$  days with Baluev (2008) false alarm probability  $\sim 1.2\%$  but cannot fully exclude other potential periods in the 4–9 day range, although all have false alarm probabilities  $\gtrsim 10\%$ . The semi-amplitude  $K_1 = 73.2 \pm 18.4 \text{ km s}^{-1}$  and  $\gamma = -36.6 \pm 9.8 \text{ km s}^{-1}$  are also uncertain due to limited sampling around phase  $\sim 0.25$ . A near-circular orbit is favoured, although other solutions with  $e \leq 0.3$  cannot be ruled out. Further observations are required to fully determine the parameters of this system.

W1050 has a candidate period of  $4.063 \pm 0.003$  days, with  $K_1 = 27.6 \pm 3.0 \text{ km s}^{-1}$ , and  $\gamma = -51.0 \pm 1.3 \text{ km s}^{-1}$ . The orbit is eccentric, with  $e = 0.56 \pm 0.10$  and  $\omega = 161 \pm 9$  degrees. We find several potential periods for W1056: the strongest candidate period is at  $53.134 \pm 0.031$  days, with  $K_1 = 28.7 \pm 3.1 \text{ km s}^{-1}$ ,  $\gamma = -41.8 \pm 1.1 \text{ km s}^{-1}$ ,  $e = 0.31 \pm 0.09$ , and  $\omega = 55 \pm 7$  degrees, although an alternative period of  $\sim 9.97$  days cannot be ruled out. This shorter period leads to very similar values of  $K_1$ ,  $\gamma$ , and  $e$ , although  $\omega \sim 0$  is required. We provisionally adopt the longer period, pending further observations. Finally, we find a period of  $3.238 \pm 0.003$  days for W1060, with false alarm probability  $< 1\%$ . The orbit is near-circular, with  $e \lesssim 0.1$ ,  $K_1 = 28.7 \pm 6.1 \text{ km s}^{-1}$ , and  $\gamma = -59.3 \pm 2.6 \text{ km s}^{-1}$ . The low semi-amplitude of these three objects suggests unfavourable inclinations and/or a low-mass companions.

### 5.7. O9 III binaries: W6b and W1063

W6b was observed on six nights in 2008–2009 and on a further three nights in 2013. Although it is classified as O9 III and is one of the faintest objects in our sample ( $I = 15.25$ ; Clark et al. 2005), the Pa-11 line is well defined and we find a candidate  $2.653 \pm 0.002$  day period, although other potential periods with  $P < 10$  days exist. The best-fit solution has  $K_1 = 41.6 \pm 4.0 \text{ km s}^{-1}$ ,  $\gamma = -64.2 \pm 2.4 \text{ km s}^{-1}$ ,  $e = 0.29 \pm 0.06$ , and  $\omega = 249 \pm 21$  degrees, with the offset

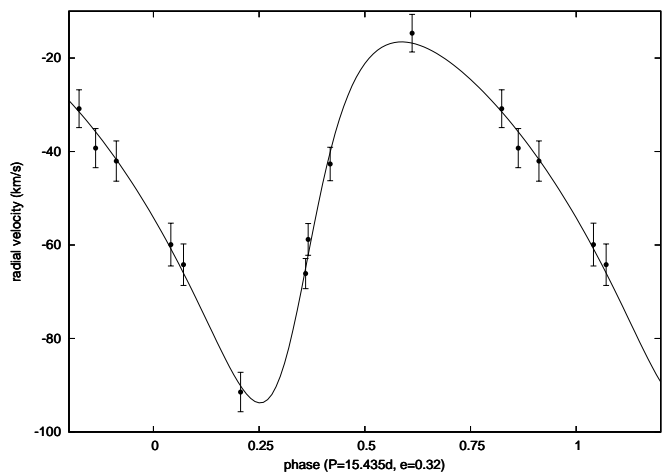


Fig. 11. RV curve for the O9.5 III star W1063.

systemic velocity suggesting we may have incomplete sampling of the full range of RVs. We caution that the solution should be considered provisional at best. There is no indication of a secondary, which we assume must still be on the MS.

W1063 displays a very similar  $I$ -band spectrum to W6b, and receives the same O9 III classification. It was observed on six nights in 2008–2009 and on a further four nights in 2013 and we find a candidate period of  $15.435 \pm 0.073$  days with  $K_1 = 38.6 \pm 2.1 \text{ km s}^{-1}$ ,  $\gamma = -47.8 \pm 1.0 \text{ km s}^{-1}$ ,  $e = 0.32 \pm 0.05$ , and  $\omega = 233 \pm 7$  degrees. The false alarm probability is  $\sim 4\%$ , although no alternative periods are identified. The wings of the Pa-11 line appear asymmetric at maximum separation, suggesting a possible contribution from an OB IV–V companion. Two low-resolution  $R$ -band spectra obtained in 2013 show  $H\alpha$  and  $\text{He I } \lambda\lambda 6678, 7065$  in absorption, with RV changes also apparent in the He I lines.

### 5.8. B2–2.5 supergiants: W2a, W23a, and W71

W23a was proposed as a candidate binary in Paper I, and was noted by Negueruela et al. (2010) as displaying *features incompatible with a single spectral type ... the spectrum may include an earlier type companion*. Our data support this assertion. W23a displays  $\text{Pa-15/Pa-16} < 1$ , a ratio that is otherwise only seen in objects earlier than B0 I (see Figure 2 in Paper III), but strong Pa-14, Pa-15, and He I  $\lambda\lambda 8845, 8777, 8583$  absorption lines *preclude* a classification earlier than B2 Ia. In addition, RVs derived from the Pa-11 and Pa-13–15 lines are in excellent agreement, with individual line centres consistent to within  $1 \text{ km s}^{-1}$ , but the Pa-16 line centre is displaced by  $\sim 30 \text{ km s}^{-1}$  (see Figure 12), with this offset and the anomalous Pa-15/Pa-16 ratio indicating blending with a strong C III  $\lambda 8500$  absorption line. The strength of this C III feature implies an  $\sim \text{O9 I}$  companion (Negueruela et al. 2010); lower luminosity classes would not be apparent in the spectrum of a highly-luminous B2 Ia primary. We note that Clark et al. (2005) highlight variable  $H\alpha$  emission from W23a, although no follow-up  $R$ -band spectra are available. If periods less than ten days are excluded as incompatible with the physical sizes of two *non-interacting* supergiants, then the string-length periodogram finds a possible period of  $\sim 40.5$  days.

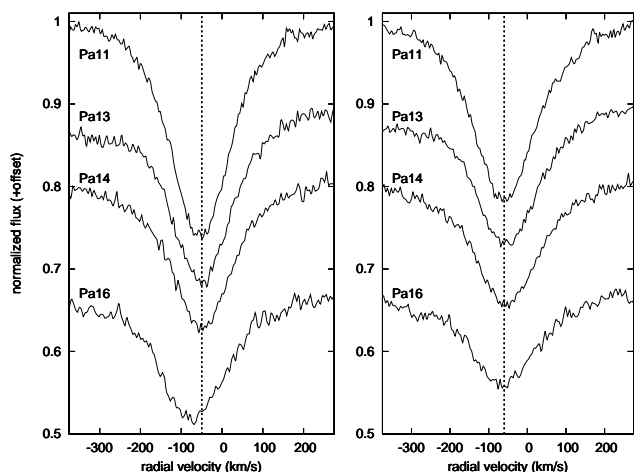


**Fig. 12.** Montage of Paschen series absorption lines in W23a (*left panel*) and W2a (*right panel*). Vertical lines mark the average of the Pa-11 and Pa-13...15 lines (Pa-12 is omitted due to the influence of the C<sub>2</sub> Phillips (2-0) system). Note the discrepant line centre and greater depth for Pa-16 in W23a due to blending with C III  $\lambda$ 8500; this is not seen in W2a or other luminous B supergiants, and implies the existence of a O9 I secondary.

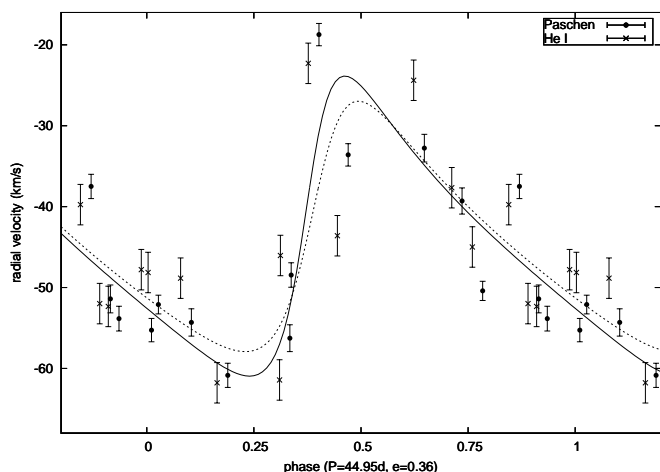


**Fig. 13.** Candidate RV curves for W2a. The solid line represents a fit to the Paschen series lines, while the dashed line represents an *independent* fit to He I  $\lambda$ 8583,8845. Scatter around the fit appears to be pulsational in origin.

We find a potential orbital solution with  $K_1 = 9.2 \pm 2.0$  and  $e \sim 0.2$ , although a circular orbit is not excluded.

Both W2a and W71 satisfy the  $\Delta RV > 25 \text{ km s}^{-1}$  cut introduced in Section 3.3, and W2a was proposed as a candidate binary in Paper I. It is not possible to fit either object with an unambiguous orbital solution, with significant residuals remaining for any choice of orbital parameters. Nevertheless, we measure a substantially higher RV amplitude in these objects than is observed in any of the other putative pulsators of similar spectral type (e.g. W8b or W57a), and these objects appear to display *both* pulsational variability and orbital motion. We tentatively identify a 44.95 day period for W2a, based on observations from both the 2008–2009 and 2013 campaigns, noting that this period

can be independently determined from both the Paschen series and from strong He I  $\lambda$ 8583,8845 absorption lines. A moderately eccentric solution ( $e \sim 0.3$ ) is preferred. Substantial scatter is present around the best-fit solution (see Figure 13), including variability on timescales of a few days that is inconsistent with a  $\sim 45$  day period, supporting the presence of both photospheric and orbital variations. Finally, we find a tentative 36.6 day solution with  $e \sim 0.1$  for W71 based off 18 epochs of data obtained during 2008–2009, with scatter again present. Neither object displays the anomalous C III  $\lambda$ 8500 absorption seen in W23a, implying secondaries in an earlier, less-luminous state.

The combination of low semi-amplitude and pulsational variability means that the candidate solutions for these three objects require additional observations for confirmation. However, with periods in the  $\sim 35$ – $45$  day range, all three objects appear potential evolutionary precursors to the interacting 53.95 day WN9h: binary W44/WR L, which is discussed further in Section 7.

### 5.9. X-ray sources: W24 and W1027

W24 (O9 Iab) is a X-ray source that is directly comparable in hardness and luminosity to the WNVL+OB binary W13 (Clark et al. 2008). The C III  $\lambda$ 8500/Pa-16 blend is variable (see Figure 4 in Clark et al. 2010), suggesting that C III  $\lambda$ 8500 may be augmented by an O-type secondary in a short-period system. W24 was observed on seven nights in 2008–2009 and a further five nights in 2013, and we find a candidate period of  $6.595 \pm 0.012$  days with false alarm probability 0.46%, although we cannot fully exclude an alternative solution with a period of 4.50 days and false-alarm probability 4.4%. The orbital solution has  $K_1 = 13.6 \pm 0.6 \text{ km s}^{-1}$  and  $\gamma = -50.4 \pm 0.4 \text{ km s}^{-1}$ : given the short period and the massive  $\sim$ O9 secondary suggested by the C III  $\lambda$ 8500 variability, this implies an almost pole-on inclination. The best fit solution has  $e = 0.25 \pm 0.04$  and  $\omega = 212 \pm 8$  degrees, implying a pre-interaction state.

W1027 (O9.5 Iab) has very similar hardness and intensity to W1040 (=C07-X3; Paper II) and W6a. It was only observed on four nights in 2013, displaying  $\Delta RV > 50 \text{ km s}^{-1}$  and change of almost  $35 \text{ km s}^{-1}$  in the space of two nights (MJDs 56494.1 and 56496.1) that confirms it as a short-period binary. Variable C III may also be present in this object, again suggesting the presence of an O9 I-II secondary, but the limited set of observations precludes determination of orbital parameters.

### 5.10. Interacting binaries: W6a, W30a, W36, and W53a

W36 (OB+OB; Negueruela et al. 2010) is a known double-lined eclipsing system ( $P = 3.18$  days; Bonanos 2007, Koumpia & Bonanos 2012), while W6a, W30a, and W53a have very strong secondary indicators of binarity, including complex, variable H $\alpha$  profiles and/or strongly enhanced X-ray emission. W30a (O4–6 Ia<sup>+</sup>) was identified as a blue straggler by Clark et al. (2019a).

W6a was classified as B0.5 Iab by Negueruela et al. (2010), and has previously been identified as a candidate binary from a 2.20 day modulation in the light curve (Bonanos 2007), variable H $\alpha$  emission, and moderate X-ray emission (Clark et al. 2008). It was observed on six nights in 2008–2009, revealing very weak and broad Paschen se-

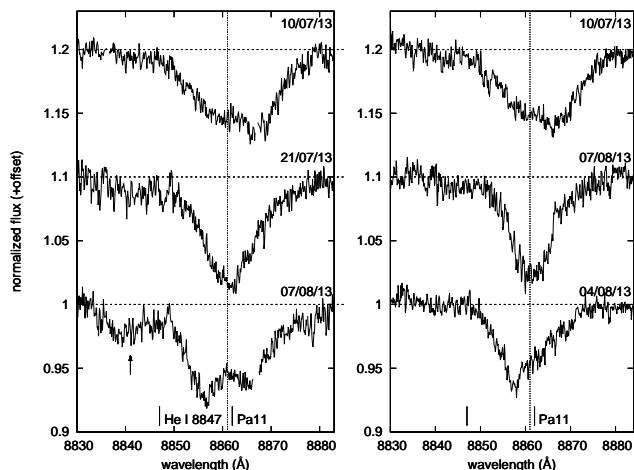


**Fig. 14.** Montage of the Pa-11 line in W36 ( $P = 3.18$  days, *Left Panel*) and W53a (*Right Panel*). Horizontal lines represent the continuum level at each epoch, and the vertical line represents the mean Pa-11 RV for stars in Westerlund 1. Spectra have been rebinned and filtered to reduce noise, and gaps indicate sky line removal as described in Section 3.2.

ries lines. Large uncertainties in fitting line profiles mean that the requirement that  $\sigma_{\text{det}} > 4$  is only just met, but RV changes with semi-amplitude  $\sim 25 \pm 5 \text{ km s}^{-1}$  confirm the binary nature of the system. No definitive period determination is possible, but we note that our minimum string length occurs at 2.217 days, consistent with the 2.20 day modulation of the light curve. Therefore, while orbital parameters cannot be confirmed, a synthesis of the RV, photometric, and X-ray data strongly suggest a very short period interacting system.

W30a was observed on eleven nights in 2008–2009, and on a further five nights in 2013. It displays  $\Delta \text{RV} > 30 \text{ km s}^{-1}$ , and although an orbital period cannot be determined with confidence, we note that a  $\sim 6.26$  day periodicity is the strongest feature in both the Lomb-Scargle periodogram and the string-length search, and suggest this may be the orbital period of the system: orbital periods above ten days appear excluded (see also discussion in Clark et al. 2019a). The semi-amplitude is very low, with  $K_1 = 13.2 \pm 2 \text{ km s}^{-1}$ , suggesting a near pole-on viewing angle or very unequal mass ratio; given the blue straggler state and high spectroscopic mass of the primary, substantial mass transfer may have occurred, leaving a low-mass, stripped secondary.

W36 was observed on five nights in 2013, fortuitously capturing the system close to both extremes of the orbit (see Figure 14). No archival  $R$ -band spectra are available. At the midpoint it appears single-lined, although the weak features appear anomalously early for its luminosity and OB Ia spectral type (Negueruela et al. 2010 and Paper III). At quadrature it is clearly double-lined, although still heavily blended. We estimate semi-amplitudes of  $K_1 = 180 \pm 20 \text{ km s}^{-1}$  and  $K_2 = 220 \pm 15 \text{ km s}^{-1}$ , consistent with the results of Koumpia & Bonanos (2012). The deeper-lined component shows greater RV changes, and we therefore associate this feature with the secondary. He I  $\lambda\lambda 8733, 8845$  absorption lines appear to be moving in phase with this component. The contact configuration (Bonanos 2007) and surprisingly low dynamical masses for its spectral type and

cluster context ( $16 + 11 M_{\odot}$ ; Koumpia & Bonanos 2012) suggest substantial mass loss has occurred in the past<sup>8</sup>. The unusual strength of He I is consistent with a secondary that has lost much of its Hydrogen envelope, and W36 appears similar to the 2.185 day overcontact binary LSS 3074 (O4f<sup>+</sup>+O6-7:(f); Raucq et al. 2017), which has evolved from a star with initial mass  $30\text{--}35 M_{\odot}$  via non-conservative Roche-lobe overflow, and is now observed in the slow-phase of Case B evolution en route to a WR+O configuration. A similar scenario for W36 would be fully consistent with the cluster environment, and would suggest W36 is an evolutionary precursor to the WN7+O binaries WR A and WR B. Further observations aimed at firmly establishing the current state and evolutionary history of W36 would be valuable.

Bonanos (2007) report W53a to be a semiregular variable with a 1.3 day periodicity in the light curve, while Clark et al. (2008) show it to be a strong X-ray source with hardness and luminosity directly comparable to W36. Observations were obtained on seven nights in 2013, including observations on consecutive nights on two occasions. Spectra show the width and profile of the Paschen series lines to vary considerably, suggesting a SB2 binary with a heavily-blended spectrum (see Figure 14) and Pa-11 line profiles vary from night to night, consistent the very short period implied by the photometric modulation. At its broadest, the spectrum appears to display two distinct minima, while at its narrowest the line centre is well defined and lies at  $-40 \pm 8 \text{ km s}^{-1}$ , close to the average systemic velocity for the cluster. We estimate  $K_1 = 125 \pm 30 \text{ km s}^{-1}$  and  $K_2 = 140 \pm 20 \text{ km s}^{-1}$ , which would imply a mass ratio  $\sim 0.9$ , noting large uncertainties in both line centres and that our limited set of observations may not fully sample the full range of RVs. If confirmed, this would support the presence of an  $\sim \text{O9 I}$  primary and  $\sim \text{O9 II}$  secondary, as suggested in Paper II. Although we cannot obtain an orbital solution from the heavily-blended  $I$ -band spectra, our results demonstrate the system is a double-lined binary and are consistent with the 1.3 day periodicity determined from the light curve. The very short orbital period precludes components later than  $\sim \text{O9 I}$  (cf. Martins et al. 2005), and the system must be in a near-contact configuration. A single low-resolution FORS spectrum is available, showing broad and weak H $\alpha$  emission and an asymmetric He I  $\lambda 7065$  absorption line. Further observations in the  $R$  band may permit a complete orbital solution to be determined.

### 5.11. Broad-lined systems: W1002, W1013, and W1021

W1021 is a 4.45 day detached, eclipsing binary first reported by Bonanos (2007). Like W53a, it was observed on seven nights in 2013, displaying an largely-featureless  $I$ -band spectrum with very broad Pa-11 and Pa-12. Although the semi-amplitudes of the two components are directly comparable to W36 (Koumpia & Bonanos 2012), the Pa-11 lines can barely be separated, and most epochs only display an asymmetric, time-varying line profile reflecting two early-type objects. Without the observations of Bonanos (2007) and Koumpia & Bonanos (2012), we could do little more than classify W2021 as a candidate O9 III-V bi-

<sup>8</sup> We note that W36 is not detected by Fenech et al. (2018) or Andrews et al. (2019), indicating current mass-loss rates are low.

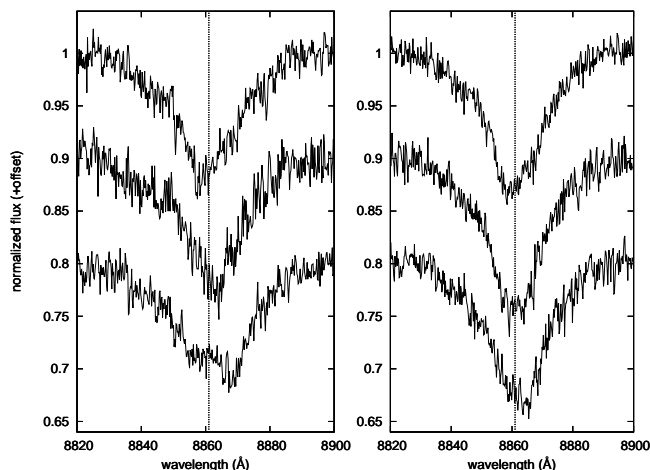


**Fig. 15.** Montage of the Pa-11 line for W1021 (=B07-DEB1,  $P = 4.45$  days, *left panel*) and W1002 (O9–9.5 II + O?, *right panel*). Vertical lines mark the mean Pa-11 RV for stars in Westerland 1. Spectra are from MJD 56483.2 (*top*), 56494.1, and 56508.1 (*bottom*), and have been rebinned and filtered to reduce noise.

nary based on its  $I$ -band morphology, with a suggestion that one component has a semi-amplitude  $\geq 150\text{km s}^{-1}$  derived from variations in the line profile. However, W2021 is important in two respects. Firstly, association of this broad-lined and time-varying  $I$ -band morphology with a confirmed early-type binary system provides support for our conjecture that many, if not all, of the systems with similar time-varying morphologies are also  $\sim$ O9 III binaries (see Section 6 and discussion Paper III). Secondly, although the Pa-11 blend is unsuitable for detailed analysis, the orbital solution provided by Koumpia & Bonanos (2012) demonstrates that follow-up observations centred on He I  $\lambda 7065$  would support determination of orbital solutions for these objects, provided that inclinations are favourable.

W1002 also displays broad lines with significant changes in line profile (see Figure 15). The  $I$ -band luminosity is similar to the O9.5 II systems discussed in Section 5.6, but broad, dilute, and asymmetric Paschen series lines are virtually identical to W1021, although the greater depth in some epochs suggests the primary has a slightly later spectral type and this system may contain an O9 II–III primary and an O-type secondary. The Paschen series lines of the two components cannot be clearly separated, but two  $R$ -band spectra are also available, with He I  $\lambda 7065$  appearing partially separated in one epoch: at least one component has a semi-amplitude  $\gtrsim 100\text{km s}^{-1}$ . We are unable to determine a potential orbital period from the available data.

Finally, W1013 is a very faint target with a similar spectrum to W1002, with broad, dilute Paschen series lines leading to an O+O? classification in Paper III. RV changes of almost  $\sim 100\text{km s}^{-1}$  appear to be present, accompanied by changes in line profile, but limited sampling and very low  $S/N$  preclude further analysis.

## 6. Candidate binaries

Alongside the targets discussed in Section 5, we find 12 systems with  $25 < \Delta RV < 50\text{km s}^{-1}$  and  $4 < \sigma_{\text{det}} < 15$ . We label these objects as *candidates* based on the

difficulty in establishing unambiguous orbital parameters with the available data: we note that significant velocity changes nevertheless make it likely that these are indeed *bona fide* binary systems, especially for the five objects with  $\Delta RV \geq 30\text{km s}^{-1}$ , which is hard to reconcile with a non-binary interpretation. Unsurprisingly, all candidates are O-type stars of luminosity class Iab–III: all B supergiants that meet the  $\Delta RV > 25\text{km s}^{-1}$  requirement also have  $\sigma_{\text{det}} > 15$ , due to their higher luminosity and narrow Paschen series lines. Only one of these candidate systems has more than ten observations, and it is therefore likely that we have not sampled the full range of RVs for these objects, especially if they have significant eccentricity: W10 and W1030 are salient examples, appearing to be an unremarkable, low semi-amplitude systems at most epochs.

### 6.1. O9–9.5 I–III systems

Four O9.5 I–III stars, one O9–O9.5 III star, and one O9 III star are identified as candidate binaries. W1018 (O9.5 Iab) is a hard X-ray source that displays a very similar  $I$ -band spectrum to W1027. RVs spanning more than  $30\text{km s}^{-1}$  appear incompatible with a non-binary interpretation, but only four epochs of data are available, precluding more detailed examination. W1042, W1043 and W1047 display strong similarities to the O9.5 II targets discussed in Section 5.6. W1042 (O9.5 II) is very likely to be binary, with a RV range of  $\sim 48\text{km s}^{-1}$ , while W1043 (O9.5 II–III) also displays RV amplitudes above  $30\text{km s}^{-1}$ , but limited observations (eight and six epochs respectively) preclude accurate determination of orbital parameters for either system. A FORS2/MXU  $R$ -band spectrum of W1043 is available, with  $H\alpha$  appearing somewhat broad and infilled compared to W1022 and W1050, although He I absorption lines appear single. W1047 (O9.5 II) was sampled on six epochs in 2008–2009 and a further four in 2013, and observations are consistent with a  $\sim 5$  day period and near-circular orbit. A FORS2/MXU spectrum shows  $H\alpha$  strongly in absorption while He I again appears single-lined. All four systems represent strong candidates for follow-up observation, which would allow robust orbital solutions to be determined.

Finally, W1026 (O9–9.5 III) and W1066 (O9 III) show broader lines that imply a lower luminosity class, with consequently increased fitting errors. W1026 displays RV changes of almost  $40\text{km s}^{-1}$ , with significant changes in line width suggesting a secondary of similar luminosity may be present. W1066 shows lower RV variability, but  $R$ -band observations of W1066 suggest He I  $\lambda 7065$  may be double. Both systems were only observed on six epochs in 2008–2009 and no further analysis can be carried out.

### 6.2. Broad-lined O-type stars

Six targets (W1001, W1006, W1017, W1028, W1029, and W1061) display broad Pa-11 and Pa-12 lines, and an otherwise featureless  $I$ -band spectrum. All are low-luminosity targets (with  $I \gtrsim 15$ ), and all are classified as O+O? or O9–9.5 III bin? in Paper III. None of these targets are detected at X-ray wavelengths (Paper II), although a FORS2/MXU spectrum of W1028 is available, with  $H\alpha$  appearing infilled and He I  $\lambda \lambda 6678, 7065$  possibly double.

All five objects display RV changes that marginally exceed our criteria for classification as *candidate* binaries, al-

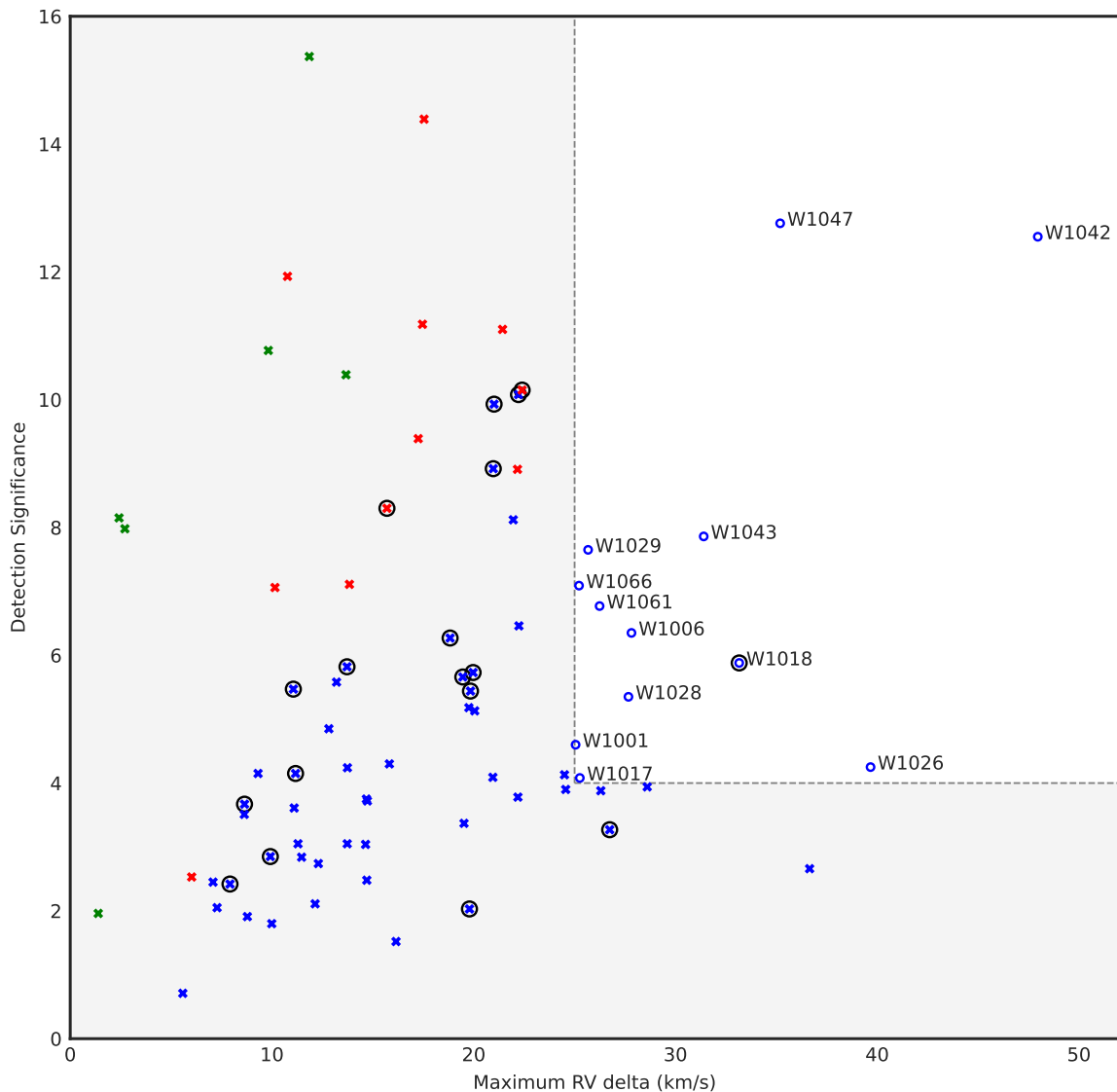


**Fig. 16.**  $\Delta RV$  vs.  $\sigma_{\text{det}}$  for *candidate* binaries. Markers follow the format of Figure 6.

though none show RV amplitudes larger than  $\sim 30 \text{ km s}^{-1}$  and all lie in the range  $4 < \sigma_{\text{det}} < 8$ . If these objects are indeed binary, then the RV changes reflect line-profile changes in heavily-blended Paschen series lines; some support for this hypothesis is given by epoch-to-epoch variations in line width in W1006, W1017, and W1061, although low  $S/N$  limits the analysis of line-profile variability. Follow-up observations at other wavelengths will be required to confirm the nature of these objects, but we note the strong morphological similarity between these systems and other confirmed binaries (e.g. W1002 or W1021) suggests that a binary interpretation is appropriate.

## 7. Wolf Rayets

The 2011 FLAMES campaign was focused on sampling the WC and WN population of Wd1, motivated by the analysis and determination of orbital parameters for W13 (WNVL) and W239/WR F (WC9d) described in Ritchie et al. (2010) and Clark et al. (2011), and the observations of W72/WR A (WN7b) and WR B (WN7o+O) presented by Bonanos (2007) and Koumpia & Bonanos (2012). This population traces the final stages of binary-mediated evolution in Wd1 from the post-interaction state (e.g. W13) to post-supernova disruption (W5/WR S).



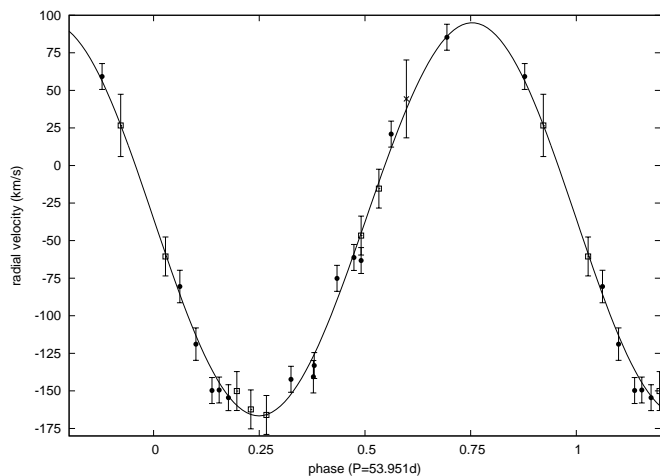


**Fig. 17.** RV curve for W44/WR L. Open squares represent VLT/FLAMES observations from 2005, 2011, and 2013, filled circles represent VLT/UVES observations from 2016, and the point labeled with an  $\times$  was derived from a low-resolution VLT/FORS spectrum obtained in 2004.

### 7.1. WN Stars

W44/WR L (WN9h; Crowther et al. 2006) was observed in HR21 mode on two nights in 2011 and four nights in 2013, with 14 epochs of data subsequently obtained with VLT/UVES in 2016. An archival FLAMES spectrum in LR8 mode from 2005 and a VLT/FORS spectrum from 2004 were also included in the analysis. RVs were measured using He I  $\lambda\lambda 8845, 8777, 8583$  absorption lines (van Helden 1972), and we find a period of  $53.952 \pm 0.004$  days, with  $K_1 = 130.8 \pm 3.7 \text{ km s}^{-1}$  and  $\gamma = -36.4 \pm 2.3 \text{ km s}^{-1}$ . The orbit is circular. W44/WR L displays dramatic emission line profile variability in H $\alpha$  and He I (Clark et al. 2010), which are a blend of static nebular emission and moving features that follow the WN9h star. The companion is not directly observed, although if we assume a  $20M_{\odot}$  mass for the emission-line object<sup>9</sup> and  $i \geq 60^{\circ}$  based on the large semi-amplitude then its mass must be  $\sim 32 - 42M_{\odot}$ . A full analysis will be presented in a forthcoming paper.

Although observations of hydrogen-rich, late-type WN stars in Wd1 have been very successful (cf. Ritchie et al. 2010; Clark et al. 2014), the remaining hydrogen-free WN stars cannot be analysed in similar detail. In HR16 mode, we only see weak lines of He I  $\lambda 7065$  in later types and N IV  $\lambda 7114$  in earlier types, but both features are broad and flat-topped, making them unsuited to RV measurement. In HR21 mode, only a weak He II line is observed, blended with a telluric band. In two cases (WR J and WR U) we observe Paschen and N I features that result from blending with nearby A-type hypergiants (W12a and W16a respectively), but we do not see any indicators of OB companions in *I*-band spectra of the remaining WN population, despite both WR A and WR U displaying strongly enhanced X-ray emission that would imply the presence of an O-type secondary.

<sup>9</sup> Crowther et al. (2006) suggest  $18M_{\odot}$  for the WN7b star WR A, while the WNVL emission-line object in W13 has a dynamical mass of  $23M_{\odot}$  (Ritchie et al. 2010).

### 7.2. WC Stars

WR H (WC9d) displays strong Paschen series absorption lines, most likely due to blending with the nearby luminous B1 Ia star W46a. WR N (WC9d) also displays weak Paschen series features superimposed on dilute C III and C IV emission lines, but is located far to the south of the cluster where blending is less likely. It is tempting to associate the Paschen series features with a massive secondary, given the expectation that an OB companion is required for dust formation (Crowther et al. 2006), but confirmation would require additional observations.

Of the other WC targets, W66/WR M (WC9d) was observed on four nights in 2011 and displays RVs spanning approximately  $100 \text{ km s}^{-1}$ , confirming it as binary, although the limited observations preclude further analysis. Variations in line profile are apparent at some epochs. W241/WR E (WC9, observed on four nights) and WR T (WC9d, observed on three nights) also display statistically-significant changes in RV, although with amplitudes below  $25 \text{ km s}^{-1}$  these cannot be distinguished from wind variability. WR C (WC9d) does not display significant variability. However, we caution that observations of these objects are very limited, and all four targets are appropriate for follow-up to extend the analysis of Clark et al. (2011).

W39b/WR K (WC8) was observed in 2008–2009 and displays no sign of orbital motion, although only very large orbital changes would be apparent in its very broad and flat-topped C III and C IV emission lines.

## 8. Late-type targets

### 8.1. Luminous B1.5–B4 supergiants

In addition to the already-discussed W2a, W23a, and W71, three other very luminous early-mid B supergiants were observed in our study, including W8b (B1.5 Ia), W70 (B3 Ia), and W57a (B4 Ia). Their high luminosity and strong Paschen series lines result in very precise RV measurement, and all three objects display substantial changes on a timescale of days, although none exceed  $\Delta RV > 25 \text{ km s}^{-1}$ . No clear periodicity or secondary indicators of binarity are present, noting the difficulty in separating low semi-amplitude motion from pulsational variability. As discussed in Paper I, these objects appear to lie in an instability strip that begins at  $\sim B0$  Ia and grows in amplitude and period towards later spectral types: we speculate that this instability may also be associated with the end of the continuous spectral sequence from O9 III to B4 Ia that we observe in Wd1, delineating a more rapid transition to the A–F hypergiant population. Given the importance of these high-amplitude pulsators in setting the RV threshold for robust identification of binary systems, further observations are required to fully characterise their pulsational behaviour.

### 8.2. The B hypergiants W1049 and W1069

W1049 and W1069 (B1-2 Ia<sup>+</sup> and B5 Ia<sup>+</sup> respectively; Paper III) are newly-identified B hypergiants associated with Wd1. The two objects were each observed on 12 epochs in 2013, with multiple observations being obtained on two nights: in these cases, measured RVs agreed to within  $1 \text{ km s}^{-1}$ . Both objects display line profile variability and low-level RV changes in the Paschen series, which are likely

due to pulsational instability, but larger RV changes indicative of a binary nature are not observed.

Both objects lie several arcminutes from the cluster core, with W1049 3'28" North of the cluster centre, and W1069 4'15" to the South East. Unlike the B1.5 Ia<sup>+</sup>/WNVL cluster member W5 (=WR S; Clark et al. 2014), neither object has a systemic velocity strongly inconsistent with the cluster mean, although W1049 shows an offset of  $\sim 15 \text{ km s}^{-1}$ . Given the suggestion that W5 is the remnant of a short-period binary system disrupted in a Type Ibc supernova (Clark et al. 2014) and the expected supernova rate in Wd1 (Paper III), it is tempting to ascribe a similar evolutionary pathway to W1049 and W1069, with Roche-lobe overflow and binary-mediated mass transfer leading to their current overluminous WNLh/B Ia<sup>+</sup> state and their ejection from the cluster in earlier supernova events.

### 8.3. A–M hypergiants

The LBV W243 was observed in both 2011 and 2013, extending the 2002–2009 baseline of observations discussed by Ritchie et al. (2009b). Classified as B2 Ia by Westerlund (1987), A2 Ia by Clark & Negueruela (2004), and A3 Ia<sup>+</sup> by Ritchie et al. (2009b), the 2013 spectra suggest a A4–5 Ia<sup>+</sup> classification based on the strength of the temperature-sensitive N I  $\lambda 8680 \dots 8686$  triplet, which now appear directly comparable to W16a (A5 Ia<sup>+</sup>; Clark et al. 2005). In addition, *I*-band Ca II and Mg I emission lines have weakened to the extent that they can be barely distinguished in 2013 spectra. The limited coverage of FLAMES in HR21 mode precludes examination of other temperature-sensitive features in the complex emission/absorption spectrum of W243.

Five YHG<sub>s</sub> were observed in 2011 or 2013. Comparison with archival FORS and FLAMES spectra from 2004–2005 precludes *significant* evolution in W4 (F3 Ia<sup>+</sup>), W12a (F1 Ia<sup>+</sup>), or W16a (A5 Ia<sup>+</sup>) during the intervening period, while W8a (F8 Ia<sup>+</sup>; Clark et al. 2005) appears as  $\sim$ F5 Ia<sup>+</sup> in 2013 spectra. W265 (F1–5 Ia<sup>+</sup>) was discussed in detail in Clark et al. (2010), with further observations in 2011 and 2013 supporting the presence of a slow pulsational cycle with quasi-period  $\sim 10^2$  days accompanied by changes in temperature-sensitive lines. However, our current baseline shows no evidence for long-term secular evolution in any of these YHG<sub>s</sub>, such as that seen in  $\rho$  Cas, HR8752, or IRC+10 420.

Finally, the RSGs W75 and W237 were observed in the 2013 campaign. W75 appears as  $\sim$ M0 Ia based on the weakness of the TiO  $\lambda 8860$  bandhead, consistent with earlier observations described by Clark et al. (2010). W237 displays a slightly stronger TiO bandhead in 2013 than in archival FLAMES observations from 2005, and we suggest a M3–4 Ia classification, noting the lower resolution of the earlier spectra. Variability is negligible over the  $\sim 4$ -week baseline of observations, with epoch-to-epoch observations in agreement to better than  $1 \text{ km s}^{-1}$ . We note that the RV of  $-47.9 \pm 0.3 \text{ km/s}$  obtained for W237 is in close agreement with the value obtained from H<sub>2</sub>O maser profiles by Fok et al. (2012).

## 9. Notable non-detections

Finally, we turn to targets that display secondary indicators of binarity, but are not identified as RV binaries or

candidate binaries. These are predominantly X-ray sources (Clark et al. 2008 and Paper II) and stars with spectral morphologies suggesting a binary nature (Paper III), but also include non-thermal radio sources (Dougherty et al. 2010, Fenech et al. 2018, and Andrews et al. 2019).

### 9.1. X-ray sources

Of all the luminous X-ray sources discussed in Paper II, only W27, an O7–8 Ia<sup>+</sup> blue straggler discussed by Clark et al. (2019a), and the WN6o star WR U (Crowther et al. 2006) are not identified as binaries or candidate binaries. As discussed in Section 7, none of our FLAMES configurations provide features suitable for RV measurement in a hydrogen-free WN star, although the strong similarities with the X-ray luminous WN7o + O stars WR A and WR B (Bonanos 2007; Clark et al. 2008) nevertheless suggest WR U is also a WN + O binary. W27 was only observed on one night in 2011 and three nights in 2013. No large excursions in RV are observed, although we note that the mean RV is offset from the cluster mean by  $\sim 20 \text{ km s}^{-1}$ , potentially indicating incomplete sampling of more significant RV changes. Secondary indicators of a binary nature include strong X-ray emission (Paper II), a complex H $\alpha$  profile, and a potentially-double He I  $\lambda 6678$  line (Negueruela et al. 2010), and this object also remains a strong binary candidate.

Although enhanced X-ray emission is a strong indicator of binarity (Skinner et al. 2006; Pittard & Dawson 2018), it is notable that few of the sources with  $L_X \sim 10^{32} \text{ erg s}^{-1}$  discussed in Paper II have been confirmed as spectroscopic binaries in this work: 17 objects do not display statistically-significant RV variability or have  $\Delta RV < 25 \text{ km s}^{-1}$ , while only W6a, W10, W24, W232, and W1027 are confirmed binaries, and W1018 is a candidate binary. Clark et al. (2008) identified eight OB supergiants with  $kT \geq 1.4 \text{ keV}$  as likely colliding-wind binaries, with two (W13 and W24) subsequently confirmed as short-period systems containing two post-MS objects (Ritchie et al. 2010 and this work). Of the remainder, W47 (O9.5 Iab) has very similar properties to W24, and was observed on three nights in 2013. W65 (O9 Ib) and W1055 (B0 Ib) are harder and less luminous sources. Both were observed on six nights in 2008–2009, while W65 was observed on a further three nights in 2013. Although all three objects display statistically-significant RV changes, none meet our  $\Delta RV > 25 \text{ km s}^{-1}$  criterion, although we caution that W47 in particular has too few observations to draw definitive conclusions; like W27, its mean RV is significantly offset from the cluster mean, again suggesting incomplete sampling. In addition, the *I*-band spectra of W65 and W1055 are suggestive of possible binarity. In the case of W65, the Paschen lines are typical of lower-luminosity O9 stars, with Pa-11 very similar to W1015 (O9 III), but the C III/Pa-16 blend is broad and weak, and the star seems rather too luminous for its early spectral type. Similarly, W1065 displays stronger C III than expected for its B0 Ib spectral type, suggesting the presence of an O-type companion. W56b (O9.5 Ib), W1036 (=C07-X4; O9.5 Ib), and W1041 (O9.5 Iab) all have  $kT \sim 1.6 \text{ keV}$  but do not display statistically-significant RV changes, although W1041 appears to be a potential binary from its *I*-band morphology and was noted as a candidate binary in Paper III. Of the X-ray sources with  $kT < 1 \text{ keV}$ , W1033 (=C07-X5; O9–9.5 I–III) and W1040 (=C07-X3; O9–9.5 I–

III) both seem somewhat too luminous for their apparent spectral type, but other objects such as W1005 (=C07-X7; B0 Iab), W1051 (O9 III), and W1064 (O9.5 Iab) show no indications of binarity other than the moderately-enhanced X-ray emission noted by Clark et al. (2008).

The lack of strong RV variability in these objects may represent unfavourable inclination rather than isolated stars, and we note that the 6.60 day hard X-ray source W24 and the X-ray luminous O4–6 Ia<sup>+</sup> interacting binary W30a also have very low semi-amplitudes, despite their massive components and compact configuration. Others may be substantially eccentric systems (cf. W10), with enhanced X-ray emission only near periastron; our survey has limited sensitivity to such a configuration, especially when only a few epochs of data are available. Alternatively, some of these objects may simply be isolated OB stars with X-ray luminosities consistent with the empirical  $L_x \sim 10^{-7} L_{\text{bol}}$  relationship, implying that X-ray detection alone is insufficient for binary classification unless emission is substantially enhanced (cf. the five OB and three WR stars with  $L_x \gtrsim 10^{33}$  erg s<sup>-1</sup> identified by Clark et al. 2008) or other binary indicators (e.g. composite spectra, or hard X-ray emission indicative of formation in a wind-collision zone) are present.

## 9.2. Morphology

With the exception of W27, which is too poorly-sampled to meet our criteria for binary classification, all of the luminous OB objects identified as candidate binaries by Negueruela et al. (2010) based on *R*- and *I*-band spectra are confirmed as binaries in this work. In contrast, Paper III identifies 25 lower-luminosity objects as candidate O-type binaries based on their *I*-band morphology (classified as either O9–9.5 III bin? or simply as O+O?), but we are only able to confirm two of these objects (W1002 and W1013) as binary in Section 5, while a third (W1021) was identified as an eclipsing binary by Bonanos (2007). A further six are identified as candidate binaries in Section 6, in every case only just exceeding the  $\Delta RV > 25$  km s<sup>-1</sup> threshold. None of these objects are listed in Paper II, suggesting they are indeed lower-luminosity objects with weak winds that cannot drive detectable X-ray emission.

The O9 III stars W6b and W1063 demonstrate that recovery of orbital properties is possible for the faintest targets in our survey, but these objects appear to have lower-luminosity OB IV–V secondaries, implying an unequal mass ratio, and appear as unblended, single-lined stars. In contrast, the morphological similarities of the broad-lined systems suggests that we may be observing a substantial population of  $\sim$ O9 III+O9 III binaries, but only those at the most favourable inclination display sufficient RV modulation to yield measurable line profile variations in their blended Paschen-series lines. Consideration of synthetic spectra suggests that orbital modulation in line profile would be sufficient to meet the criteria in Section 3.3 for  $i \gtrsim 60^\circ$  and  $P \lesssim 10$  days, but the broad Paschen series lines in a short-period O9 III+O9 III system would remain heavily blended, precluding recovery of orbital parameters. Our ability to accurately measure RV changes in these objects using the Paschen series lines is therefore very limited. The high reddening towards Wd1 means that alternative photospheric lines are largely unavailable, although studies of

He I $\lambda$ 7065 represent a potential route forward with these objects (cf. Koumpia & Bonanos 2012).

## 9.3. Radio sources

Dougherty et al. (2010) reported non-thermal emission from two targets, W15 (O9 Ib) and W17 (O9 Iab), although Fenech et al. (2018) report detecting only W17. In addition, radio emission from W1031 (O9 III) and W1056 (O9.5 II) is reported by Andrews et al. (2019). W15, W17, and W1031 do not meet the criteria for classification as candidate binaries, although observations are limited to only six or seven epochs, and in all three cases statistically-significant RV changes are present with amplitudes  $\sim 20$  km s<sup>-1</sup>, close to our threshold for classification. Our observations are therefore consistent with the suggestion that these systems are all long-period and potentially eccentric binaries (Andrews et al. 2019) that may be hard to detect conclusively in an RV survey unless viewed at favourable inclination. W1056 is the only OB star that is both a radio detection and a confirmed binary, and although its orbital parameters are not yet secure, our provisional period of 53.1 days with  $e \sim 0.3$  would be in good agreement with such a scenario. The status of W1030, another long period, eccentric system that likely contains an O9 Ib (or possibly B0 Ia) primary and post-MS secondary is uncertain: it lies outside the coverage reported by Andrews et al. (2019), and is not detected by Fenech et al. (2018).

## 10. Discussion

### 10.1. Sensitivity

This initial study of Wd1 with VLT/FLAMES has demonstrated the challenge of detecting binary systems in the cluster. High reddening precludes the use of standard diagnostic lines in the blue region of the spectrum, particularly the strong He I, He II, and Si III lines covered by FLAMES setups LR02–LR03 and HR02–HR06, and we are forced to rely on Paschen series lines in setup HR21. These are most effective for single-lined  $\sim$ O9.5 II–B0 Ia systems, where luminosity (and hence  $S/N$ ) is increasing rapidly but pulsational variability is less pronounced. Although the Paschen lines are very strong in later types, disentangling orbital and pulsational variability becomes increasingly challenging, while early-type systems suffer from broad lines and low  $S/N$ . We have very limited sensitivity to double-lined systems at any spectral type, as separation of the Paschen series lines requires the system to have a large semi-amplitude, coupled in some cases with fortuitous timing (e.g. W10). We would expect the supergiant population to skew towards SB1s, as the high luminosity of the primary would imply the secondary is undetectable unless the mass ratio is close to unity and both systems are in a similar evolutionary state. Double-lined systems become much more likely at lower luminosity classes, and it is likely that we are observing a large population of heavily blended SB2s in the O9 III population. We briefly summarise our sensitivity as follows:

- At short orbital periods ( $P < 5$  days), the most massive stars will have already undergone Roche-lobe overflow, and even under favourable inclinations our ability to separate the Paschen series lines in short-period interacting systems (e.g. W36 or W53a) is very limited.

**Table 5.** Binaries in Westerlund 1, with orbital solutions where available. Errors are omitted to save space, but are given in the text or in the cited references. Values where the orbital period is candidate or tentatively identified are marked with one (candidate) or two (tentative) question marks, while other parameters with errors  $\geq 20\%$  are also highlighted with a question mark.

ID	Spectral Type	Type <sup>†</sup>	$P$ (days)	$K_1$ (km s <sup>-1</sup> )	$K_2$ (km s <sup>-1</sup> )	$\gamma$ (km s <sup>-1</sup> )	$e$	$\omega$ (degrees)
W2a	B2 Ia	SB1	44.95??	18.5	-	-44.6	~ 0.3?	285?
W6a	B0.5 Iab	SB1/P, X	2.21?	25?	-	-38.9	0	-
W6b	O9.5 III	SB1	2.65??	41.6	-	-64.2	0.29?	249?
W10	B0.5 Ia + O9.5 II	SB2, X	-	75?	85?	-34.7	$\geq 0.3?$	0?
W23a	B2 Ia + O9 I	SB1*	40.46?	9.2?	-	-52.5	~ 0.2?	220?
W24	O9 Iab + O9 I?	SB1*, X	6.60?	13.6	-	-50.4	0.25?	212
W30a	O4-6 Ia <sup>+</sup> + O	SB1, X	6.3?	13?	-	-42.3	0	-
W36 <sup>a,b</sup>	OB + OB	SB2/E, X	3.18	175	235	-37	0	-
W43a	B0 Ia	SB1	16.23	69.4	-	-64.4	0.10	149
W52	B1.5 Ia	SB1/P	6.62?	24.7?	-	-48?	0?	-
W53a	O + O	SB2/P, X	1.3	125?	140?	-40?	0	-
W71	B2.5 Ia	SB1	36.64??	9.8	-	-44.8	~ 0.1?	90?
W232	B0 Iab	SB1	9.98	14.7?	-	-45.3	0.41	256?
W1021 <sup>a,b</sup>	O + O	SB2/E	4.45	229	187	-40	0.18	252
W1022	O9.5 II	SB1	6.18?	73.2?	-	-36.6?	$\leq 0.3?$	-
W1030	O9.5 Ib	SB1	173.85	16.5	-	-46.6	0.56	323
W1048	O9.5 Ib	SB1/E?	8.75	76.2	-	-64.0	0.08	205
W1050	O9.5 II	SB1	4.06?	27.6?	-	-51.0	0.56?	161
W1056	O9.5 II	SB1	53.13?	28.7	-	-41.8	0.31	55?
W1060	O9.5 II	SB1	3.24	28.7?	-	-59.3	$\leq 0.1?$	-
W1063	O9 III + O?	SB1	15.44?	38.6	-	-47.8	0.32?	233
W1065	B0 Ib	SB1	11.13	52.8	-	-39.4	0.38	256
W1067	B0 Ib	SB1	6.13	13.2?	-	-46.9	0.52?	0?
W13 <sup>a,b,c</sup>	WNVL + OB	SB2/E, X	9.27	210.2	137.3	-48.2	0	-
WR A / W72 <sup>a</sup>	WN7b + O?	P, X	7.63	-	-	-	-	-
WR B <sup>a,b</sup>	WN7o + O?	SB1/E, X	3.52	-	360	-35	0	-
WR F / W239 <sup>d</sup>	WC9d + O + ?	SB1	5.05	39.7	-	-60.5	0	-
WR L / W44	WN9h: + O?	SB1	53.95	130.8	-	-36.4	0	-

Notes: <sup>†</sup>Listed as Single/Double lined (**SB1**/**SB2**) and **E**clipsing or **P**eriodic photometric variables. Strong **X**-ray sources are also noted (Clark et al. 2019a). \*The influence of C III $\lambda$ 8500 absorption originating in a luminous O9 secondary is apparent, but lines from the secondary cannot be observed directly, and the object is therefore listed as an SB1.

References: <sup>a</sup>Bonanos (2007), <sup>b</sup>Koumpia & Bonanos (2012), <sup>c</sup>Ritchie et al. (2010), <sup>d</sup>Clark et al. (2011).

- Pre-interaction systems may be found at  $\sim$ O9.5 II and earlier (e.g. W1021 or W1050), and orbital parameters can be recovered if the system is an SB1.
- Sensitivity peaks for SB1s with spectral types in the range O9.5 II to B0 Ia and periods  $5 < P \lesssim 15$  days. Such systems represent an optimum balance of relatively high luminosity, narrow Paschen series features, lower pulsational instability, and orbital periods that make it likely that we will obtain reasonable sampling of the full RV curve. The majority of systems identified as binary fall in this range.
  - At longer orbital periods ( $P > 20$  days), sensitivity drops rapidly and a large number of observations are required to separate orbital and photospheric variability; it is also increasingly likely that we do not have full sampling of the full range of RVs. Objects later than  $\sim$ B1 Ia require wider orbits to accommodate the primary, but growing pulsational instability requires favourable inclination and/or a luminous secondary (cf. W23a) to unambiguously support a binary interpretation.
  - At  $P \gtrsim 100$  days sensitivity is very low, with W1030 representing an almost ideal case of favourable spectral type (O9.5 Ib) and a relatively large number of observations spanning a five-year baseline. We would be unable to conclusively detect this object at earlier or later spectral types.
  - We have limited sensitivity to systems with high eccentricity, which is reflected in the lack of any robust solutions with  $e \gg 0.5$ . RVs may be below the  $\Delta RV > 25 \text{ km s}^{-1}$  cut for much of the orbit in highly-eccentric systems, and even when a discrepant RV near periastron confirms the object as a binary, the orbital solution will be unreliable unless the periastron passage is well sampled.
- Many of the identified binary and candidate binary systems exceed  $\Delta RV > 25 \text{ km s}^{-1}$  in the 2008–2009 dataset alone, implying that a  $\Delta RV$  cut can effectively detect (candidate) binaries even if the number of epochs of observation is low. However, the additional RV data and extended baseline of observations provided by the 2011 and 2013 observations

**Table 6.** Candidate Binaries in Wd1, listing indicators of binarity: RV changes, X-Ray Luminosity, Infra-Red Excess, Non-thermal Radio Emission, Spectral Morphology (e.g. Double Lines, Broad Lines, or anomalously Weak Lines). Indicators that are strongly inconsistent with a single star are shown as solid circles, while indicators that suggest a binary interpretation are shown as open circles. Objects are listed if they (a) display substantial RV changes ( $\Delta RV > 25 \text{ km s}^{-1}$ ), (b) display any single secondary indicator strongly inconsistent with a single star, or (c) display two or more indicators that individually suggest binarity.

ID	Spectral Type <sup>a</sup>	Radial Velocity	X-Ray <sup>b</sup>	Infra-Red	Radio	Morphology
W9	sgB[e]		●	● <sup>c</sup>	○ <sup>c</sup>	
W15	O9 Ib		○		○ <sup>d</sup>	
W17	O9 Iab	○	○		● <sup>d</sup>	
W27	O7–8 Ia <sup>+</sup>	○	●			
W47	O9.5 Iab	○	○			
W65	O9 Ib	○	○			○
W1001	O + O?	●				○
W1002	O9 II–III + O?	●				●
W1006	O9–9.5 III bin?	●				○
W1013	O + O?	●				○
W1017	O9–9.5 III bin?	●				○
W1018	O9.5 Iab	●	○			
W1026	O9–9.5 III	●				
W1027	O9.5 Iab	●	○			○
W1028	O9–9.5 III bin?	●				○
W1029	O9–9.5 III bin?	●				○
W1031	O9 III		○		○ <sup>e</sup>	
W1033	O9–9.5 I–III		○			○
W1040	B0 Iab		○			○
W1041	O9.5 Iab + ?		○			○
W1042	O9.5 II	●				
W1043	O9.5 II–III	●				
W1046	O + O?					● <sup>g</sup>
W1047	O9.5 II	●				
W1055	B0 Ib (+O?)		○			○
W1061	O9–9.5 III bin?	●				○
W1066	O9 III	●				●
WR C	WC9d			● <sup>f</sup>		
WR H	WC9d			● <sup>f</sup>		
WR M	WC9d + O?	●		● <sup>f</sup>		
WR N	WC9d		○	● <sup>f</sup>		○
WR T	WC9d			● <sup>f</sup>		
WR U	WN6o		●			

References: <sup>a</sup>Clark et al. (2020), <sup>b</sup>Clark et al. (2019b), <sup>c</sup>Clark et al. (2013), <sup>d</sup>Dougherty et al. (2010), <sup>e</sup>Andrews et al. (2019), <sup>f</sup>Crowther et al. (2006), <sup>g</sup>Paper III.

greatly supported determination of orbital parameters, and few of the objects discussed in Section 5 had robust solutions based on just the 2008–2009 dataset.

### 10.2. Cumulative Distribution of orbital periods

Figure 18 plots a preliminary cumulative distribution function (CDF) of orbital periods for Wd1, with the sample of Galactic O stars from Sana et al. (2012) plotted for comparison, noting that we include candidate periods and make no attempt to correct for bias, and further work is required before this result can be considered robust. Nevertheless, Wd1 appears to share the overabundance of short-period systems noted in other massive clusters (e.g. Sana & Evans 2011; Kobulnicky et al. 2014; Almeida et al. 2017), while the very steep gradient of the CDF between 5–15 days reflects the peak sensitivity in this range noted in the pre-

vious section. The CDF flattens above  $\sim 50$  days as a result of our insensitivity to long period systems. We tentatively note an apparent lack of very short-period systems compared to Sana et al. (2012), and note that all of the luminous objects with  $P \lesssim 5$  days are interacting systems (e.g. W6a, W36, or W53a) or post-interaction systems (e.g. WR-B or W239/WR F). At a cluster age of  $\sim 5$  Myr (Negueruela et al. 2010) any massive ( $\gtrsim 40 M_{\odot}$ ) binaries with very short orbital periods will have already undergone Roche-lobe overflow (e.g. Wellstein et al. 2001; Petrovic et al. 2005). At lower masses, very short period systems will still be in a pre-interaction state, but will be heavily blended unless observed at favourable inclination, and only a handful of early-type systems have confirmed (W1021, W1060) or candidate (W6b, W1050) periods below five days.

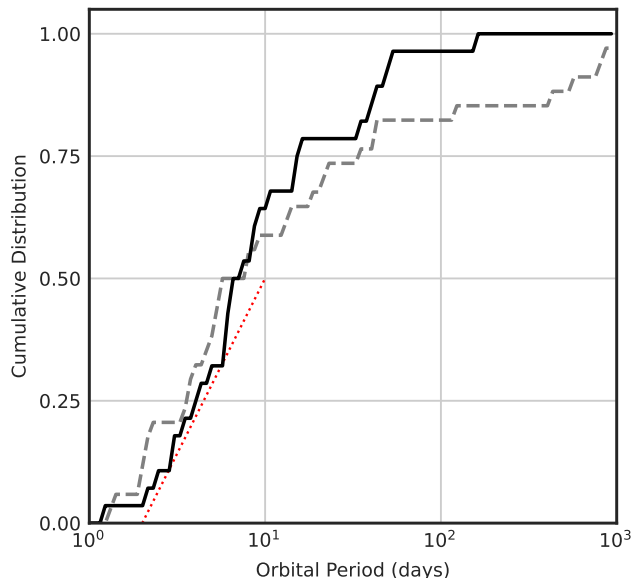


**Fig. 18.** Preliminary cumulative distribution of orbital periods from the OB stars in this work (solid line) and O stars in galactic clusters (Sana et al. 2012; dashed line). The dotted line shows the expected distribution if half the binary systems have a period in the range 2–10 days (Sana & Evans 2011).

### 10.3. The OB Binary Fraction in Westerlund 1

Of the 166 confirmed cluster members listed in Paper III, 133 are OB stars, with spectral types ranging from  $\sim$ O9 III to B9 Ia<sup>+</sup>; of the remainder, 22 are Wolf-Rayets, while 11 are cool-phase hypergiants. We report 26 OB binaries in Section 5, while Section 6 adds a further 12 objects; although we classify these as *candidates* due to the challenge of extracting orbital parameters, they exceed the  $\Delta RV > 25 \text{ km s}^{-1}$  cut and are very likely to be binary (see also Sana et al. 2013; Simón-Díaz et al. 2020; Lohr et al. in prep.). We estimate incompleteness due to unfavourable inclination at  $\sim 10\%$  in Section 3.3. Collectively, this suggests a minimum binary fraction in the OB population of  $\sim 40\%$ , consistent with the initial assessment in Paper I. This value is below the O star binary fraction of  $69 \pm 9\%$  in Galactic open clusters (Sana et al. 2012), but slightly higher than the spectroscopic binary fraction of  $\sim 35\%$  reported for 30 Dor by Sana et al. (2013), which corresponds to objects displaying  $\Delta RV > 20 \text{ km s}^{-1}$ . A true binary fraction of 51% is inferred, although Almeida et al. (2017) suggests  $\sim 60\%$  may be more appropriate.

Several factors could increase our estimated binary fraction in Wd1. Firstly, a substantial population of broad-lined O9 III objects were proposed as binary in Paper III, and evidence presented here supports this conjecture: if confirmed, the binary fraction must be in excess of 50%. Secondly, we have very limited sensitivity to long period, eccentric, or unequal-mass binary systems, and have identified only one system with  $P \gg 50$  days and none with  $e \gg 0.5$ . If we assume that Wd1 follows other Galactic clusters (cf. Sana et al. 2012), then we would expect a significant number of currently-undetected systems, even at

favourable spectral type. Thirdly, some objects have very limited sampling and do not meet the  $\Delta RV > 25 \text{ km s}^{-1}$  cut based on the available data, but display an offset mean RV or epoch-to-epoch variability that suggests that additional observations would confirm their binary nature. Other OB cluster members have no multi-epoch observations at all. Finally, we have objects with very strong secondary indicators of binarity, such as the sgB[e] star W9, the blue straggler W27, or the non-thermal radio source W17, that have not been confirmed as RV binaries in this paper.

Although there is overlap between these categories, they collectively suggest that binary fraction might even approach the  $\sim 70\%$  inferred for the WR population (Crowther et al. 2006). However, an equivalence would be surprising, as the Wolf-Rayet population is believed to be shaped by binary-mediated evolution, and we caution that the target selection discussed in Paper I may be biased towards binary systems, while the 2011 and 2013 datasets preferentially select candidate systems for follow-up observations. A conclusive determination of the cluster binary fraction must therefore await a future programme of work that provides a substantial baseline of observation across an unbiased sample of cluster objects.

### 10.4. Binary Interaction

Figure 19 plots the orbital period of confirmed and candidate binary systems against their *I*-band magnitude, which serves as a crude proxy for evolutionary state. Systems with zero and non-zero eccentricity are plotted separately. Although a circular orbit does not necessarily imply a post-interaction state, almost all targets with  $P < 10$  days and  $e = 0$  are either interacting systems (W6, W30a, W36, or W53a) or post-interaction Wolf-Rayet binaries (W13, W72/WR A, WR B, or W239/WR F). The evolutionary state of W52 is unclear: given its high luminosity, a short period and circular orbit suggest a post-interaction system, but *R*-band spectroscopy shows an unremarkable B1.5 Ia supergiant with weak H $\alpha$  emission, while He I is in absorption; the post-interaction early-B/WNVL objects W5/WR S and W13 display very different spectra with strong H $\alpha$  and He I emission. Further observations are required to determine its state. W1060 is a less-evolved O9.5 II star with a very short period.

Given that most luminous ( $I < 14$ ), short-period ( $P < 10$  days) systems have circular orbits, W24 (O9 Iab+O9 I?) and W1067 (B0 Ib) stand out for retaining significant eccentricity; lack of circularisation in the short-period O9 II-III systems with *I*-band magnitudes fainter than 14 is less surprising, as these less-evolved systems are not yet expected to interact, while W1048 (O9.5 Ib) has  $e < 0.1$ . W1067 displays H $\alpha$  emission with a weak P Cygni profile, which is unusual for its spectral type and suggests a potentially-interacting system, while the 6.6 day candidate period and near-equal mass ratio of W24 also implies that the primary must be close to Roche-lobe overflow. W24 may therefore be a direct precursor to the sgB[e] W9 (Clark et al. 2013), which is currently observed in the fast phase of Case A mass transfer. We speculate that the system may then emerge in a similar configuration to W36 or W53a, which are directly comparable in *I*-band and X-ray luminosity. The lack of a robust period for W10 makes its state less certain; most potential periodicities are greater than ten days, but shorter periods are not yet ruled out. If it has  $P < 10$  days then it

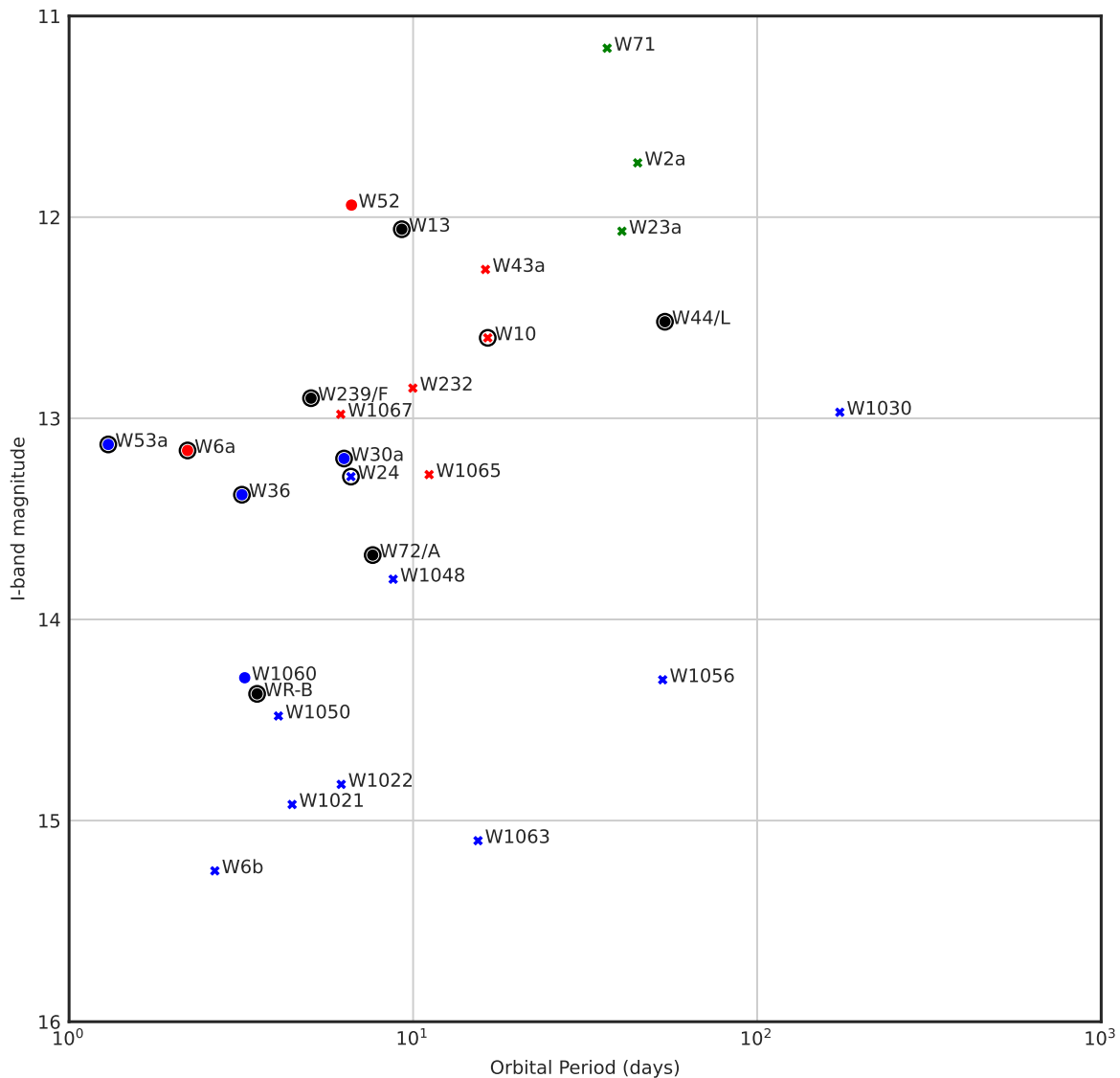


**Fig. 19.** Orbital period vs.  $I$ -band magnitude for target with photometry from Clark et al. (2005) or Bonanos (2007). Systems with circular orbits are plotted as filled circles, while systems with eccentric orbits are plotted with ‘x’ symbols. Black circles show X-ray sources from Paper II. Red, green, and blue points indicate spectral type, following Figures 6 and 16. Note that the orbital period for W10 is not firm, and its  $I$ -band magnitude is estimated from its  $R$ -band magnitude of 18.516 (Bonanos 2007) under the assumption that it has the same reddening as other nearby early-B supergiants.

must also be close to Roche-lobe overflow and circularisation.

At longer periods ( $P > 10$  days), all OB stars in our sample have non-zero eccentricity. W44/L is the only longer-period object with a circular orbit, and is clearly an interacting system that may represent the next evolutionary stage of the luminous B2 Ia supergiants

W2a, W23a, and W71. We examine W44/L further in Ritchie et al. (in prep.).

Finally, Figure 19 demonstrates the selection effects discussed previously. W1030 is the only system with  $P > 100$  days, reflecting our lack of sensitivity to longer-period systems, but there is also a general lack of lower-luminosity systems (i.e.  $I$ -band magnitudes fainter than  $\sim 13$ , corresponding to objects earlier than  $\sim O9.5$  II) with  $P >$

10 days. The low  $S/N$ , broad lines, and low semi-amplitude of such systems make direct confirmation of binarity impossible with our current data. Similarly, there is a lack of very luminous, short period systems. Such objects have already undergone binary interaction, and are now represented in the binary-rich Wolf-Rayet population or as disrupted, post-supernova systems: the early-mid B hypergiants W5, W1049, and W1069 may be examples of the latter evolutionary endpoint.

### 10.5. Future Observations

Finally, we turn to future observations of Wd1. The HR21 mode of FLAMES works well for targets of spectral type O9.5 II and later, and further observations would support the discovery of additional long period and high-eccentricity systems, and would allow refinement of the initial solutions presented here. W10, W24, W52, and WR M are of particular importance in this respect, as they mark the entry and exit points of the short-period binary evolutionary channel in Wd1, while the potential eclipsing system W1048 may place constraints on the masses of systems entering the luminous B supergiant phase.

HR21 mode is less effective for the lower-luminosity O9 III population, and future programmes should also target the He I  $\lambda 7065$  absorption line covered by FLAMES HR16 and LR6 modes. Although HR16 mode proved unsuitable for detecting RV variability in the WN population, spare fibres were allocated to a few bright supergiants, including W10 and W56a, and demonstrated that high quality observations of He I  $\lambda 7065$  can be obtained. However, no fainter targets were observed and the performance of this mode at low  $S/N$  cannot be assessed. LR6 covers H $\alpha$  and He I  $\lambda \lambda 6678, 7065$ , and approximately half of our sample was observed in this mode. He I  $\lambda 7065$  remains well defined down to O9 III in many cases, and appears better-defined than Pa-11 in the faintest targets. Some confirmed binaries discussed in Section 5 were observed twice in LR6 mode, and observations of W1063 (O9 III) demonstrate that He I  $\lambda 7065$  may be used to measure RVs in the faintest objects in our target list. Our only observations of W36 and W1021 are in the  $I$ -band, but we note that Koumpia & Bonanos (2012) successfully measured RVs for these objects from He I  $\lambda 7065$ . However, the line is broad and weak in the majority of objects classified O9-9.5 III bin? or O+O? in Paper III, suggesting blending is still present. Nevertheless, LR6 and HR16 modes appear a promising route forward for future observations of Wd1, although their performance requires further assessment.

## 11. Conclusions

In this paper, we have presented multi-epoch observations of more than 100 OB and Wolf-Rayet stars in the massive Galactic cluster Westerlund 1. We summarise our findings as follows:

1. We find OB binaries with spectral types that range from B2 Ia to O9 III, with the 173.9 day eccentric system W1030 representing the first longer-period binary detected in the cluster. W10 and W53 are confirmed as SB2s, although both require follow-up observations to determine robust orbital solutions, while the simultaneous presence of He I and C III in the spectrum of W23a is inconsistent with an isolated star and implies a B2 Ia+O9 I binary. Several other objects display signs of composite spectra, most commonly in the anomalous strength of C III  $\lambda 8500$ .
2. W232 appears unique in displaying two distinct and stable periodicities, with one exactly 11 times the other, indicating the presence of tidally-excited oscillations in a 9.98 day eccentric system: it may be a massive ‘heart-beat’ star (Fuller 2017). This object is unusually well sampled, and other examples may be found in future observations, especially if contemporaneous RV and photometric data become available.
3. Twelve candidate OB binaries are identified. Five display  $\Delta RV > 30 \text{ km s}^{-1}$ , but only limited observations are available, precluding further analysis: additional data will likely confirm these systems as binary. In addition, a number of other poorly-sampled objects are not currently identified as candidate binaries, but show secondary indicators of binarity or have mean RVs offset from the cluster mean, suggesting incomplete sampling of the RV curve. Additional observations of these objects may also confirm their (candidate) binary nature.
4. Pulsational instability appears to grow from O9 II to B2 Ia, and a lower RV cut might be appropriate for luminosity class II-III. We have not examined a varying RV cut in this paper, which would require a better understanding of pulsational instability in these objects, but note that adopting a  $\Delta RV > 20 \text{ km s}^{-1}$  cut for our O9.5 II - O9 III targets would increase the number of candidate binaries by  $\sim 50\%$ .
5. Many of the faintest targets in our survey display broad, flat-bottomed Paschen series line profiles, with Paper III proposing that these systems are heavily blended double-lined systems. We find evidence to support this hypothesis, but in most cases cannot confirm the binary nature of these systems: only a few objects with this broad-lined morphology display RV changes large enough for conclusive classification as spectroscopic binaries.
6. A number of objects have been identified as strong binary candidates in previous X-ray (Clark et al. 2008) or radio (Dougherty et al. 2010; Fenech et al. 2018) observations, but could not be confirmed here. In some cases this may reflect insufficient observations (e.g. the strong X-ray source W27), but may also be a result of unfavourable inclination; in a large sample, we would expect some objects with very strong secondary indicators of binarity to be viewed at an angle that results in negligible RV variability.
7. Amongst the Wolf-Rayet population, we find an orbital solution for the 53.95 day WN9h: binary W44/WR L and detect large RV changes in the WC9d star WR M, extending the list of Wolf-Rayet stars with massive, unseen companions in Wd1. W44/WR L is the first longer-period Wolf-Rayet binary identified in the cluster, and likely represents a different evolutionary pathway to the  $P < 10$  day WR+O? systems W72/WR A, WR B, and W239/WR F (Bonanos 2007; Clark et al. 2011).
8. Almost all luminous binary systems with  $P < 10$  days appear to be interacting. The hard X-ray source W24 (O9 Iab+O9 I?) has a candidate period of 6.595 days but shows no apparent sign of binary interaction; if confirmed, this system must be near the onset of Roche-lobe overflow, and may be a direct precursor to the X-ray luminous sgB[e] star W9 (Clark et al. 2013). We



do not find any very luminous binaries ( $I < 13$ ) with  $P < 5$  days.

9. All OB binaries with  $P > 10$  days have non-zero eccentricity and appear to be pre-interaction systems: the B2 Ia+O9 I binary W23a may represent an evolutionary precursor to W44/WR L. The apparent lack of X-ray luminous systems with longer periods is likely a selection effect: as discussed in Paper II, X-ray detections peak at O9–9.5 I, but as orbital periods increase such systems become increasingly difficult to confirm as binary.
10. Although it is too early to attempt a robust determination of the OB binary fraction in Wd1, our results provide direct confirmation that the cluster is binary-rich, as suggested by earlier multiwavelength studies (Crowther et al. 2006; Clark et al. 2008). A preliminary estimate suggests a binary fraction in excess of  $\sim 40\%$ , consistent with other massive clusters (Sana & Evans 2011). However, our survey is optimised for short-period systems, and our understanding of the population of longer-period binaries is very limited: future observations of Wd1 may therefore significantly raise this estimate.

*Acknowledgements.* The authors thank the referee for helpful comments and suggestions that have clarified this paper. Based on observations collected at the European Southern Observatory under programme IDs ESO 081.D-0324, 383.D-0633, 087.D-0440, and 091.D-0179. This research is partially supported by the Spanish Government Ministerio de Ciencia, Innovación y Universidades under grant PGC2018-093741-B-C21 (MICIU/AEI/FEDER, UE). I.N. is also supported by the Generalitat Valenciana through grant PROMETEO/2019/041. F.N. acknowledges financial support through Spanish grant PID2019-105552RB-C41 (MINECO/MCIU/AEI/FEDER) and from the Spanish State Research Agency (AEI) through the Unidad de Excelencia "María de Maeztu"-Centro de Astrobiología (CSIC-INTA) project No. MDM-2017-0737.

## References

- Almeida, L.A., Sana, H., Taylor, W., et al. 2017, *A&A*, 598, 84  
 Andrews, H., Fenech, D., Prinja, R.K., Clark, J.S. & Hindson, L. 2019, *A&A*, 632, A38  
 Baluev, R.V. 2008, *MNRAS*, 385, 1279  
 Bonanos, A.Z. 2007, *AJ*, 133, 2696  
 Bosch, G., Terlevich, E., & Terlevich, R. 2009, *AJ*, 137, 3437  
 Clark, J.S. & Negueruela, I. 2004, *A&A*, 413, L15  
 Clark, J.S., Negueruela, I., Crowther, P.A. & Goodwin, S. 2005, *A&A*, 434, 949  
 Clark, J.S., Muno, M.P., Negueruela, I., et al. 2008, *A&A*, 477, 147  
 Clark, J.S., Ritchie, B.W. & Negueruela, I. 2010, 514, A87  
 Clark, J.S., Ritchie, B.W. & Negueruela, I., et al. 2011, *A&A*, 531, A2  
 Clark, J.S., Ritchie, B.W. & Negueruela, I. 2013, *A&A*, 560, A11  
 Clark, J.S., Ritchie, B.W. & Najarro, F., Langer, N. & Negueruela, I. 2014, *A&A*, 565, A90  
 Clark, J.S., Negueruela, I., Ritchie, B.W., et al. 2015, *The Messenger*, 159, 30  
 Clark, J.S., Najarro, F., Negueruela, I., et al. 2019a, *A&A*, 623, A83  
 Clark, J.S., Ritchie, B.W. & Negueruela, I. 2019b, *A&A*, 626, A59 (Paper II)  
 Clark, J.S., Ritchie, B.W. & Negueruela, I. 2020, *A&A*, 635, A187 (Paper III)  
 Crowther, P.A., Hadfield, L.J., Clark, J.S., Negueruela, I. & Vacca, W.D. 2006, *MNRAS*, 372, 1407  
 Damiani, A., Almeida, L.A., Blum, R.D., et al. 2016, *MNRAS*, 463, 2653  
 Dougherty, S.M., Clark, J.S., Negueruela, I., Johnson, T. & Chapman, J.M. 2010, *A&A*, 511, A58  
 De Becker, M. & Raucq, F. 2013, *A&A*, 558, A28  
 Dworetzky, M.M., 1983, *MNRAS*, 203, 917  
 Evans, C.J., Hunter, I., Smartt, S.J., et al. 2008, *The Messenger*, 131, 25  
 Evans, C.J., Lennon, D.J., Langer, N., et al. 2020, *The Messenger*, 181, 22  
 Fenech, D.M., Clark, J.S., Prinja, R.K., et al. 2018, *A&A*, 617, A137  
 Fok, T.K.T., Nakashima, J., Yung, B.H.K., Hsia, C-H, & Deguchi, S. 2012, *ApJ*, 760, 65  
 Fuller, J. 2017, *MNRAS*, 472, 1538  
 Kobulnicky, H.A., Kiminki, D.C., Lundquist, M.J., et al. 2014, *ApJS*, 213, 34  
 Koumpia, E. & Bonanos, A.Z. 2012, *A&A*, 547, A30  
 Langer, N., Wellstein, S. & Petrovic, J. 2003, in: *IAU Symp. 212, A Massive Star Odyssey, from Main Sequence to Supernova*, eds. van der Hucht, K.A., Herrero, A., & Esteban, C., 275  
 Lohr, M.E., Clark, J.S., Najarro, F., et al. 2018, *A&A*, 617, A66  
 Lomb, N.R. 1976, *Ap&SS*, 39, 447  
 Mahy, L., Lanthermann, C., Hutsemékers, et al. 2021, *A&A* in press (arXiv:2105.12380)  
 Martins, F., Schaerer, D., & Hillier, D.J. 2005, *A&A*, 436, 1049  
 Negueruela, I., Clark, J.S. & Ritchie, B.W. 2010, *A&A*, 516, A78  
 Pasquani, L., Avila, G., Blecha, A., et al. 2002, *The Messenger*, 110, 1  
 Petrovic, J., Langer, N. & van der Hucht, K.A. 2005, *A&A*, 435, 1013  
 Pittard, J.M. & Dawson, B. 2018, *MNRAS*, 477, 5640  
 Porter, A., Blundell, K., Podsiadlowski, P., & Lee, S. 2021, *MNRAS*, 503, 4802  
 Price-Whelan, A.M., Hogg, D.W., Foreman-Mackey, D., & Rix, H.-W. 2017, *ApJ*, 837, 20  
 Raucq, F., Gosset, E., Rauw, G., et al. 2017, *A&A*, 601, A133  
 Ritchie, B.W., Clark, J.S., Negueruela, I. & Crowther, P.A. 2009a, *A&A*, 507, 1585 (Paper I)  
 Ritchie, B.W., Clark, J.S., Negueruela, I. & Najarro, F. 2009b, *A&A*, 507, 1597  
 Ritchie, B.W., Clark, J.S., Negueruela, I. & Langer, N. 2010, *A&A*, 520, A48  
 Ritchie, B.W., Clark, J.S. & Negueruela, I. 2011, *Bulletin de la Société Royale des Sciences de Liège*, 80, 628  
 Sana, H., Gosset, E., Nazé, Y., Rauw, G. & Linder, N. 2008, *MNRAS*, 386, 447  
 Sana, H. & Evans, C.J. 2011, *Proceedings of the International Astronomical Union*, 6(S272), 474  
 Sana, H., de Mink, S.E., de Koter, A., et al. 2012, *Science*, 337, 444  
 Sana, H., de Koter, A., de Mink, S.E., et al. 2013, *A&A*, 550, A107  
 Scargle, J.D. 1982, *ApJ*, 263, 835  
 Schneider, F.R.N., Izzard, R.G., Langer, N. & de Mink, S.E., 2015, *ApJ*, 805, 20  
 Simón-Díaz, S., Britvaskiy, N., Castro, N. & Holgado, G. 2020, *Contributions to the XIV.0 Scientific Meeting (virtual) of the Spanish Astronomical Society*.  
 Skinner, S.L., Simmons, A.E., Zhekov, S.A., et al. 2006, *ApJ*, 639, L35  
 Stevens, I.R., Blending, J.M. & Pollock, A.M.T. 1992, *ApJ*, 386, 265  
 van Helden, R. 1972, *A&A*, 19, 388  
 Wellstein, S., Langer, N. & Braun, H. 2001, *A&A*, 369, 939  
 Westerlund, B.E. 1961, *PASP*, 73, 51  
 Westerlund, B.E. 1987, *A&AS*, 70, 311  
 Willems, B. & Aerts, C. 2002, *A&A*, 384, 441  
 Williams, P.M., van der Hucht, K.A., Morris, P.W. & Marang, F. 2003, in: *IAU Symp. 212, A Massive Star Odyssey, from Main Sequence to Supernova*, eds. van der Hucht, K.A., Herrero, A., & Esteban, C., 115

**Table 8.** Summary of Radial Velocity observations. Binaries listed in Table 5 are shown in **bold**, and candidate binaries listed in Table 6 are shown in *italics*.

ID	Spectral Type	Observations	P(null)	Mean RV (km s <sup>-1</sup> )	RV Range (km s <sup>-1</sup> )	Mean Error (km s <sup>-1</sup> )	$\sigma_{\text{det}}$
W1	O9.5 Iab	6	0.000	-59.26	11.17	1.91	4.15
<b>W2a</b>	B2 Ia	14	0.000	-46.06	42.12	0.46	55.91
<b>W6a</b>	B0.5 Iab	7	0.000	-38.90	40.21	9.72	4.03
<b>W6b</b>	O9.5 III	9	0.000	-57.17	84.38	2.58	20.92
W8a	F8 Ia <sup>+</sup>	5	0.000	-46.55	2.71	0.24	7.98
W8b	B1.5 Ia	11	0.000	-47.85	16.18	0.35	39.26
<b>W10</b>	B0.5 I + O9.5 II	10	0.000	-58.16	149.69	1.24	68.39
W12a	F1 Ia <sup>+</sup>	5	0.000	-44.71	9.82	0.65	10.77
<i>W15</i>	O9 Ib	6	0.000	-44.81	19.46	1.98	5.66
W16a	A5 Ia <sup>+</sup>	3	0.000	-40.60	11.85	0.56	15.37
<i>W17</i>	O9 Iab	7	0.000	-36.87	22.22	1.52	10.08
W21	B0.5 Ia	11	0.000	-46.58	24.36	1.11	16.75
<b>W23a</b>	B2 Ia + O9 I	11	0.000	-50.78	18.94	0.52	25.91
<b>W24</b>	O9 Iab + O9 I?	12	0.000	-51.14	26.60	1.76	15.05
<i>W27</i>	O7-8 Ia <sup>+</sup>	4	0.000	-60.56	13.20	1.03	5.58
<b>W30a</b>	O4-6 Ia <sup>+</sup>	16	0.000	-41.27	34.17	4.27	5.37
W37	O9 Ib	6	0.000	-46.02	21.96	1.77	8.12
W38	O9 Iab	6	0.000	-44.19	21.01	1.48	9.93
W41	O9 Iab	3	0.000	-49.50	20.97	1.10	8.92
<b>W43a</b>	B0 Ia	11	0.000	-65.24	145.47	0.93	117.76
<i>W47</i>	O9.5 Iab	3	0.000	-58.08	19.97	1.75	5.73
W49	B0 Iab	6	0.000	-38.11	13.84	1.29	7.11
W50b	O9 III	7	0.004	-36.10	13.73	3.12	3.05
<b>W52</b>	B1.5 Ia	5	0.000	-43.68	37.96	0.71	37.27
W55	B0 Ia	18	0.000	-47.85	21.43	1.27	11.10
W56a	B1.5 Ia	6	0.000	-55.37	19.70	0.63	29.82
W56b	O9.5 Ib	6	0.001	-44.53	12.82	1.76	4.85
W57a	B4 Ia	7	0.000	-53.13	12.06	0.32	23.13
W60	B0 Iab	11	0.000	-40.71	17.25	1.37	9.39
<i>W65</i>	O9 Ib	9	0.000	-46.74	18.83	2.30	6.27
W70	B3 Ia	6	0.000	-42.86	17.73	0.38	31.46
<b>W71</b>	B2.5 Ia	18	0.000	-44.89	29.37	0.50	45.95
W74	O9.5 Iab	6	0.000	-45.90	11.06	1.24	5.47
W75 <sup>a</sup>	M4 Ia	4	0.238	-50.02	1.39	0.51	-
W78	B1 Ia	11	0.000	-45.99	20.49	0.61	23.44
W84	O9.5 Ib	14	0.000	-49.40	19.84	2.09	5.44
W86	O9.5 Ib	6	0.010	-50.94	8.63	1.85	3.51
W228b	O9 Ib	6	0.000	-45.21	22.24	2.68	6.46
<b>W232</b>	B0 Iab	36	0.000	-48.95	50.01	1.76	20.42
W237 <sup>a</sup>	M3 Ia	8	0.000	-47.86	2.42	0.21	-
W238	B1 Iab	7	0.000	-43.46	17.54	0.84	14.39
W243 <sup>b</sup>	A3 Ia <sup>+</sup>	20	0.000	-34.08	24.33	0.23	76.46
W265	F1-5 Ia <sup>+</sup>	19	0.000	-49.24	14.05	0.35	27.16
W373	B0 Iab	11	0.000	-47.29	17.46	0.97	11.18
<i>W1001</i>	O + O?	6	0.000	-42.43	25.05	3.36	4.60
<b>W1002</b>	O9-9.5 II + O?	10	0.000	-58.12	66.00	5.57	8.43
W1003	O9-9.5 bin?	6	0.000	-45.63	20.95	3.48	4.09
W1005	B0 Iab	15	0.000	-34.61	22.40	1.44	10.15
<i>W1006</i>	O9-9.5 III bin?	8	0.000	-54.32	27.82	3.02	6.35
W1007	O9-9.5 III	6	0.024	-46.13	7.08	1.86	2.45
W1008	O9.5 II	6	0.333	-47.05	7.28	2.77	2.05
W1009	B0 Ib	6	0.000	-40.80	6.02	1.92	2.53
W1010	O + O?	6	0.069	-53.27	36.65	7.73	2.66
W1011	O + O?	7	0.005	-48.11	22.19	4.18	3.78
W1012	O9-9.5 III bin?	6	0.001	-40.49	25.00	5.18	4.13
<b>W1013</b>	O + O?	6	0.000	-57.40	98.82	7.32	6.86
W1014	O9-9.5 III bin?	6	0.002	-41.18	19.52	4.60	3.37

Table 8. continued.

ID	Spectral Type	Observations	P(null)	Mean RV (km s <sup>-1</sup> )	RV Range (km s <sup>-1</sup> )	Mean Error (km s <sup>-1</sup> )	$\sigma_{\text{det}}$
W1015	O9 III	6	0.006	-40.19	14.73	2.77	3.72
W1016	O9-9.5 III bin?	6	0.012	-44.21	14.64	3.89	3.04
W1017	O9-9.5 III bin?	9	0.000	-53.76	25.26	4.00	4.08
W1018	O9.5 Iab	4	0.000	-46.86	33.16	3.99	5.88
W1019	O9-9.5 III bin?	7	0.002	-47.45	26.30	4.36	4.18
W1020	O9-9.5 + O?	6	0.003	-44.49	14.68	2.82	3.75
<b>W1022</b>	O9.5 II	10	0.000	-34.87	122.69	2.83	33.19
W1023	O9 III	7	0.059	-49.94	11.47	2.42	2.84
W1024	O9.5-B0 Ib	6	0.001	-43.47	9.41	1.70	4.15
W1025	O + O?	6	0.186	-41.22	16.15	5.90	1.52
W1026	O9-9.5 III	9	0.000	-37.85	39.76	4.26	5.25
<b>W1027</b>	O9.5 Iab	4	0.000	-40.97	50.22	2.97	13.16
W1028	O9-9.5 III bin?	9	0.000	-48.97	27.67	4.40	4.76
W1029	O9-9.5 III bin?	6	0.000	-43.27	25.67	2.82	6.81
<b>W1030</b>	O9.5 Ib	22	0.000	-46.77	34.81	1.72	13.02
W1031	O9 III	7	0.000	-39.70	20.05	2.58	5.13
W1032	O9-9.5 III bin?	7	0.001	-37.88	28.60	4.80	4.34
W1033	O9-9.5 I-III	6	0.161	-43.70	7.92	2.29	2.42
W1034	O9.5 Iab	1	-	-49.06	-	2.16	-
W1035	O9-9.5 III bin?	11	0.000	-39.57	24.56	4.12	3.90
W1036	O9.5 Ib	13	0.266	-30.89	9.92	2.50	2.85
W1037	O9.5 II	6	0.295	-39.44	8.78	3.46	1.91
W1038	O9 III	6	0.000	-40.47	13.74	2.57	4.24
W1039	B1 Ia	6	0.000	-45.52	10.77	0.70	11.93
W1040	O9.5 Iab	6	0.000	-49.25	13.72	1.55	5.82
W1041	O9.5 Iab bin?	5	0.285	-46.80	19.79	6.90	2.03
W1042	O9.5 II	8	0.000	-36.55	47.96	2.80	12.55
W1043	O9.5 II-III	6	0.000	-49.67	31.40	3.24	7.86
W1044	O9.5 III?	7	0.151	-38.47	12.14	4.48	2.11
W1045	O9.5 II	6	0.008	-40.27	11.29	2.71	3.05
W1046	O + O?	6	0.057	-44.01	12.30	3.03	2.74
W1047	O9.5 II	10	0.000	-46.65	35.19	1.84	12.76
<b>W1048</b>	O9.5 Ib	9	0.000	-82.16	151.24	2.23	43.23
W1049	B1-2 Ia <sup>+</sup>	12	0.000	-59.67	22.43	0.69	24.18
<b>W1050</b>	O9.5 II	11	0.000	-56.36	54.26	2.65	14.81
W1051	O9 III	6	0.003	-39.32	8.64	1.77	3.67
W1052	O9 III	3	0.741	-41.00	5.58	5.06	0.71
W1053	B0 Ib	3	0.000	-46.99	10.15	0.97	7.06
W1054	O9-9.5 bin?	6	0.004	-45.95	11.10	2.40	3.61
W1055	B0 Ib	6	0.000	-35.66	15.70	1.40	8.30
<b>W1056</b>	O9.5 II	10	0.000	-44.65	51.06	2.27	16.86
W1057	O9.5 Ib	9	0.001	-41.43	19.76	2.86	5.18
W1058	O9 III	6	0.000	-45.75	15.82	2.57	4.30
W1059	O9 III?	6	0.445	-39.62	9.99	4.23	1.80
<b>W1060</b>	O9.5 II	10	0.000	-54.63	56.92	3.02	11.40
W1061	O9-9.5 III bin?	10	0.000	-37.67	26.24	2.96	6.77
W1062	O + O?	6	0.019	-45.99	14.70	4.10	2.48
<b>W1063</b>	O9 III	10	0.000	-51.01	76.77	2.70	18.68
W1064	O9.5 Iab	3	0.005	-51.20	26.74	5.79	3.27
<b>W1065</b>	B0 Ib	27	0.000	-35.53	79.47	1.02	44.60
W1066	O9 III	6	0.000	-37.20	25.22	2.49	7.09
<b>W1067</b>	B0 Iab	17	0.000	-47.75	29.02	0.89	25.53
W1068	B0 Ib	6	0.000	-30.83	22.17	2.20	8.91
W1069	B5 Ia <sup>+</sup>	12	0.000	-43.23	13.67	0.88	10.39
<b>W13<sup>c</sup></b>	WNVL + OB	11	0.000	-48.20	292.0	9.45	32.80
<b>WR C<sup>d</sup></b>	WC9d	4	0.084	-67.10	7.79	3.23	1.39
WR E (W241) <sup>d</sup>	WC9	4	0.000	-78.74	17.66	2.16	7.73
<b>WR F (W239)<sup>d</sup></b>	WC9d	11	0.000	-60.50	70.40	3.51	14.22

**Table 8.** continued.

ID	Spectral Type	Observations	P(null)	Mean RV (km s <sup>-1</sup> )	RV Range (km s <sup>-1</sup> )	Mean Error (km s <sup>-1</sup> )	$\sigma_{\text{det}}$
<b>WR L (W44)</b> <sup>e</sup>	WN9h: + O?	6	0.000	-63.73	150.65	2.82	62.16
<b>WR M (W66)</b> <sup>d</sup>	WC9d + O?	4	0.000	-63.41	102.71	2.58	28.18
WR S (W5)	WN10-11h	6	0.000	-97.65	7.82	0.69	7.50
<b>WR T</b> <sup>d</sup>	WC9d	3	0.000	-57.28	22.33	2.18	6.12

Notes:

<sup>a</sup>RVs measured from Ca II $\lambda$ 8542,8662. Epoch-to-Epoch variability < 1km s<sup>-1</sup>.<sup>b</sup>RVs measured from Ca II $\lambda$ 8912,8927 (see Ritchie et al. 2009b).<sup>c</sup>Values given for the more massive absorption-line components (Ritchie et al. 2010).<sup>d</sup>RVs measured from the C III  $\lambda$ 8664 emission line (see Clark et al. 2011).<sup>e</sup>RVs measured from He I  $\lambda$ 8845. Values presented for 2011 and 2013 FLAMES observations only.

